UNIVERSIDAD NACIONAL AUTÓNOMA DE MÉXICO
PROGRAMA DE MAESTRÍA Y DOCTORADO EN INGENIERÍA
ENERGÍA – ENERGÍA Y MEDIO AMBIENTE

COMPARATIVE ANALYSIS ASSISTED BY COMPUTATIONAL FLUID DYNAMICS (CFD) OF THE ECONOMIC AND SIMPLIFIED BOILING WATER REACTOR (ESBWR) PASSIVE COOLING SYSTEMS CONSIDERING NANOFLUIDS ADDITION

TESIS
QUE PARA OPTAR POR EL GRADO DE:
DOCTOR EN INGENIERÍA

PRESENTA:
GALLARDO VILLARREAL JOSÉ MANUEL

TUTOR PRINCIPAL
DR. JAIME B. MORALES SANDOVAL, FI

COMITÉ TUTOR
DR. JUAN LUIS FRANÇOIS LACOUTURE, FI
DRA. CECILIA MARTÍN DEL CAMPO MÁRQUEZ, FI
DR. AUGUSTO HERNÁNDEZ SOLIS, KTH
M. EN I. WAYNE MARQUINO, GEH

CIUDAD UNIVERSITARIA, CD MX, ENERO 2018

JURADO ASIGNADO:

Presidente: **DR. JUAN LUIS FRANÇOIS LACOUTURE**

Secretario: **DRA. CECILIA MARTÍN DEL CAMPO MÁRQUEZ**

Vocal: **DR. JAIME B. MORALES SANDOVAL**

1 er. Suplente: **M. EN I. WAYNE MARQUINO**

2 d o. Suplente: **DR. AUGUSTO HERNÁNDEZ SOLIS**

Lugar o lugares donde se realizó la tesis: **CIUDAD UNIVERSITARIA, CD MX**

TUTOR DE TESIS:

DR. JAIME B. MORALES SANDOVAL

FIRMA

(Segunda hoja)

Acknowledgements

To my Mom and sister for their understanding

To professor Morales for his never ending guide

To the other members of the doctoral committee for their patience

To Emilio for the shared journey

To Clau's family for their support

To Clau for everything

Contents

Abstract

Water evaporation and boiling exhibit different dynamics in time and space that are essential in determining long-term evolutions of mass and energy in heated water bodies. In chapter 1 experiments with a localized heat source and different boundary conditions are analyzed using temperature evolutions, evaporation rates, and separate dimensionless quantities in the process of model verification and validation. With a combined Reduced Order Model – Computational Fluid Dynamics analysis it is found that the heat transfers through the water-air surface with or without mass transport are the most significant dissipation mechanisms. Finally, a simple evaporation analysis is concluded to be a viable approach for configurations with power densities of less than 100 kW/m³.

In chapter 2 the nanofluids impact in heat transfer mechanisms due to convection and conduction effects, as well as during phase change is analyzed through the implementation of TiO_2 and Al_2O_3 nanofluids properties in CFD and a thermal-hydraulic two phase 1D-transient model based on TRAC-BF1 routines. TRAC-U is introduced as a systematic and ongoing attempt to incorporate new developments into TRAC-BF1. The analysis uses the optimized model developed for chapter 1 and a model developed in TRAC-U. It is found that the impact on the system depends on the dominant mechanism of heat transfer. The density appears to be the most significant parameter in both models considering the five properties modified in the implementation of nanofluids.

In chapter 3 the results from chapter 1 and chapter 2 as well as an additional set of first principles experiments are used to draw conclusions about possible enhancements to the ESBWR passive cooling systems. It is found that losing coolant by evaporation is preferable over a pool with a near-complete inventory at higher temperature. A passive TPCT cooled by air that removes decay heat while conserving the water inventory of the PCCS pools coupled with a shroud favoring the phase change around the heat exchangers seems like the optimal alternative to enhance the ESBWR passive cooling

systems. Limiting cases probably bounding the PCCS actual response when adding nanofluids are identified.

Resumen

La evaporación y ebullición del agua exhiben dinámicas diferentes en el tiempo y en el espacio que son esenciales para determinar la evolución a largo plazo de la masa y la energía en cuerpos de agua calentados. En el capítulo 1 experimentos con una fuente de calor localizada y diferentes condiciones de frontera son analizados usando evoluciones de temperatura, tasas de evaporación y distintas cantidades adimensionales en el proceso de verificación y validación del modelo. Con un análisis combinado de un Modelo de Orden Reducido y Dinámica Computacional de Fluidos se encontró que las transferencias de calor a través de la superficie agua-aire con o sin transporte de masa son los mecanismos de disipación más significativos. Finalmente, se concluye que un simple análisis de evaporación es viable para configuraciones con densidades de potencia menores a 100 kW/m^3.

En el capítulo 2 el impacto de los nanofluidos en los mecanismos de transferencia de calor debido a efectos de convección y conducción, así como durante el cambio de fase es analizado a través de la implementación de las propiedades de nanofluidos de TiO_2 y Al_2O_3 en CFD y un modelo termohidráulico 1D de 2 fases transitorio basado en las rutinas de TRAC-BF1. TRAC-U es introducido como un esfuerzo sistemático y continuo de incorporar nuevos desarrollos en TRAC-BF1. El análisis usa el modelo optimizado desarrollado para el capítulo 1 y el modelo desarrollado en TRAC-U. Se encontró que el impacto en el sistema depende del mecanismo dominante de transferencia de calor. La densidad parece ser el parámetro más significativo en ambos modelos considerando las cinco propiedades modificadas en la implementación de los nanolfuidos.

En el capítulo 3 los resultados del capítulo 1 y 2 así como un conjunto adicional de experimentos basados en primeros principios son usados para llegar a conclusiones acerca de posibles mejoras a los sistemas de refrigeración pasiva del ESBWR. Se encontró que perder refrigerante por evaporación es preferible a una piscina con un inventario casi completo a mayor temperatura. Un TPCT enfriado por aire que remueva el calor de decaimiento mientras conserva el inventario de agua de las piscinas del PCCS junto a una camisa favoreciendo el cambio de fase alrededor de los

intercambiadores de calor parece ser la alternativa óptima para mejorar los sistemas de refrigeración pasiva del ESBWR. Se identifican casos extremos que probablemente acotan la respuesta real del PCCS al agregar nanofluidos.

Acronyms and Nomenclature

Acronyms

CFD	Computational Fluid Dynamics
ESBWR	Economic and Simplified Boiling Water Reactor
ROM	Reduced Order Model
TPCT	Two Phase Closed Thermosyphon
TRAC-U	Transient Reactor Analysis Code – UNAM

Nomenclature

m	mass, kg
t	time, s
C_P	specific heat capacity at constant pressure, J/(kg*K)
T	temperature, °C
$\dot{Q}$	transferred power, W
h	heat transfer coefficient, W/(m^2*K)
A	area, m^2
H	height, m
$f(u)$	generalized wind function
$g(P)$	generalized pressure function
$h(T)$	generalized temperature function
L	latent heat, J/kg

Greek symbols

$\in$	emissivity

σ	Stefan-Boltzmann constant, 5.67×10^{-8} W/(m²*K⁴)
ρ	density, kg/m³
λ	temperature constant, °C
η	weight variable for wind function
τ	time constant, s

Subscripts

in	power source
r	radiation
c	convection
v	evaporation
b	boiling
amb	ambient
$surf$	surface (plastic or water)
$wall$	plastic wall
0	initial condition
L	loss
$Floor$	plastic floor
W	plastic *wall (temperature)*
max	maximum
air	air (temperature)
eq	equilibrium
V	vapor

L   *liquid*

Superscripts

W   *water*

P   *plastic*

Introduction

The objective of the current investigation is to find possible enhancements to the ESBWR passive cooling systems, including the possibility of adding nanofluids.

The original hypothesis was that adding nanofluids would reduce the peak temperature or lead to faster cooling in comparison with the case where the emergency systems were not augmented. The investigation was rooted on the outstanding properties reported in the literature for certain configurations with nanofluids.

Nevertheless, along the progress of the investigation project several limitations were identified. Namely, the proprietary nature of the information about the passive cooling systems, the inconsistency in the literature about the enhancement or deterioration due to nanofluids, the significant computational power required to model a two-phase 3D transient, among others.

Several approaches were tried in order to circumvent these limitations, including: (a) purchasing ZnO nanoparticles in an attempt to acquire first-hand experience with nanoparticles, (b) trying several CFD models of different complexity in order to find a practical yet insightful approach, and (c) designing first principles experiments to identify the main heat transfer mechanisms for different boundary conditions applicable to the passive cooling systems.

With all this experience, the final approach consisted of (1) estimating in detail the heat transfer mechanisms in an experimental prototype similar to a scaled-down passive cooling system, using a Reduced Order Model assisted by Computational Fluid Dynamics, (2) analyzing the nanofluids impact in heat transfer mechanisms due to convection and conduction effects and during phase change (Introducing TRAC-U), and (3) studying first principles experiments to gain insight into the effects in the evaporation rate of different passive cooling systems configurations, expanding the alternatives to enhance the ESBWR passive cooling systems beyond nanofluids.

The next chapters, each one representing a scientific article, follow closely this approach, listing concluding remarks specific to each activity. Finally, the last chapter collects the major findings reached during the doctoral project.

Estimation of Heat Transfer Mechanisms in Heated Water Bodies Using a Reduced Order Model Assisted by Computational Fluid Dynamics

Abstract

Water evaporation and boiling exhibit different dynamics in time and space that are essential in determining long-term evolutions of mass and energy in heated water bodies. In the present study experiments with a localized heat source and different boundary conditions are analyzed using temperature evolutions, evaporation rates, and separate dimensionless quantities in the process of model verification and validation. With a combined Reduced Order Model – Computational Fluid Dynamics analysis it is found that the heat transfers through the water-air surface with or without mass transport are the most significant dissipation mechanisms. Finally, a simple evaporation analysis is concluded to be a viable approach for configurations with power densities of less than 100 kW/m³.

1 Introduction

The phase change of a liquid substance into vapor is usually described indistinctly as evaporation or boiling, particularly when the substance of interest is water. However, water evaporation and boiling exhibit different dynamics in time and space that are essential in determining long-term evolutions of mass and energy in heated water bodies.

According to *Çengel and Boles* [1] "a liquid-to-vapor phase change process is called evaporation if it occurs at a liquid–vapor interface, and boiling if it occurs at a solid–liquid interface". In addition to the interface, other relevant differences between these processes are the speed of the phase change, the formation of bubbles, the bulk temperature of the system and the source supplying the required energy. Specifically, evaporation is a gradual phenomenon that takes place when the vapor pressure in the air is less than the saturation pressure at the liquid surface temperature, does not present bubble formation, the bulk temperature of the system is below the boiling point, and does not require an external energy source.

Therefore, evaporation and boiling must be accurately predicted for optimal evaluations of the inter-relationship between humans and water resources. This is particularly true when the analysis is constrained by time, computational power or other restrictions, whether the application is the design of industrial equipment or the prediction of natural systems.

Computational Fluid Dynamic (CFD) analyses tend to only provide meaningful insight when the phenomena studied can be narrowed down to the scope of specific well-known models or when there is experimental data that allows to validate the simulations. However, even in those cases, these calculations might not be practical for long-term predictions in the presence of two phase flows, sudden transients or even detailed three dimensional geometries. In situations of that kind, and if there is also enough data to verify or validate the underlying assumptions, the use of specific simple relationships or reduced order models (ROM) may help provide the required answers.

The present study is part of a larger research project described in Figure 1, where experiments with a localized heat source and different boundary conditions are analyzed using temperature evolutions, evaporation rates, and separate dimensionless quantities in the process of model verification and validation [2]. Additionally, the ratio of supplied power to water volume in the system, referred as power density in this analysis, is considered as a figure of merit to study the system and globally predict the transition in evaporation between local boiling and non-local boiling.

The objectives of this paper are (1) to identify the main heat transfer rates taking place in a heated water body and (2) to evaluate in terms of power dissipation and mass loss if ROMs with support from first principles mathematical models and experimental data collected in this study can predict the long-term response of a system involving boiling and evaporation due to a localized heat source. With a combined ROM-CFD analysis this paper provides an approach particularly useful for modeling water systems involving a multiphase process of different time and space scales.
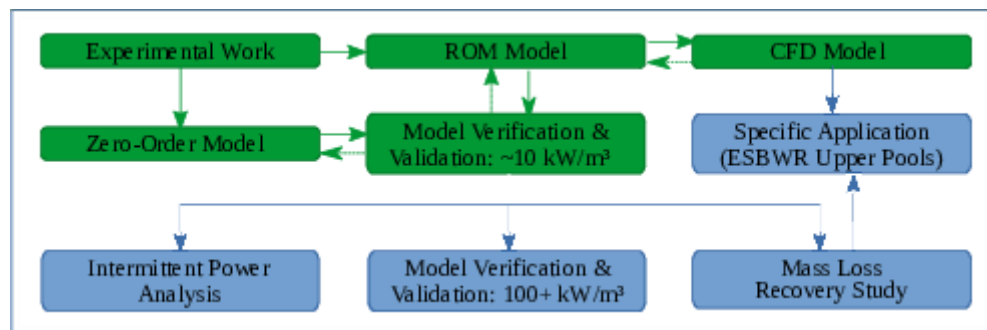

Fig. 1 General structure of the research project encompassing the present study. Iterative processes are represented with dotted lines, complete stages in green and pending stages in blue

2. Methods

2.1 System configuration

Two configurations were used during this study. The first one was designed to investigate the impact of boundary conditions in an evaporation system with a volume of 190 dm³ and a submerged electrical resistance with an approximate power of 1600 W as external energy source. These parameters were chosen to allow a water volume loss of 50% in a period of 72 hours without uncovering the electrical resistance.

The experiments with this configuration were conducted at 77 and 85 kPa. The temperature was registered at three separate levels and three radial locations as detailed in Figure 2 trying to detect local temperature variations as shown in Figure 3 for the experimental data and Figure 4 for the CFD simulation, and keeping track of the surface water level throughout the experiment. Power was monitored through the supplied voltage and current to avoid significant variations in the energy source of the system. The data acquisition interface was implemented with Arduino and open source software as summarized in Figure 5.
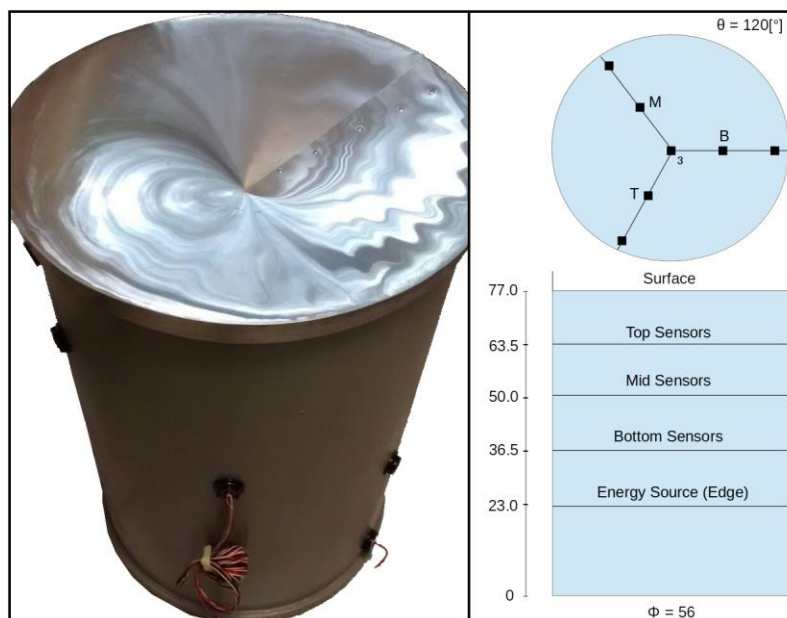

Fig. 2 Evaporation experiment first configuration with 190 dm³ (All length units in cm)

Different boundary conditions for this configuration were examined as part of this study while keeping constant the power supplied to the system. The impact of reducing fluid loss due to evaporation at the cost of increasing vapor pressure was analyzed by adding a lid to the container close to the surface, with and without a fin submerged in the water body. The effect of fast heat removal in the container lid was also considered by using a fan to cool its external surface.

The second configuration of the evaporation experiment displayed in Figure 6 consisted of a small-scale system with a volume of 0.6 dm³ at a pressure of 77 kPa, where the power supplied was varied to study the effect of the power density. Experimental data for this configuration was collected until at least half the volume was evaporated. The only exception was the case run with a power density of about 1 kW/m^3, that was ended after 72 hours.

No substances or additives were added to the water in any of the configurations, although *Wong and De Leon* [3] show that suspensions of nanoparticles in fluids, or simply nanofluids, have a wide range of possible applications to enhance the heat transfer even at modest concentrations.

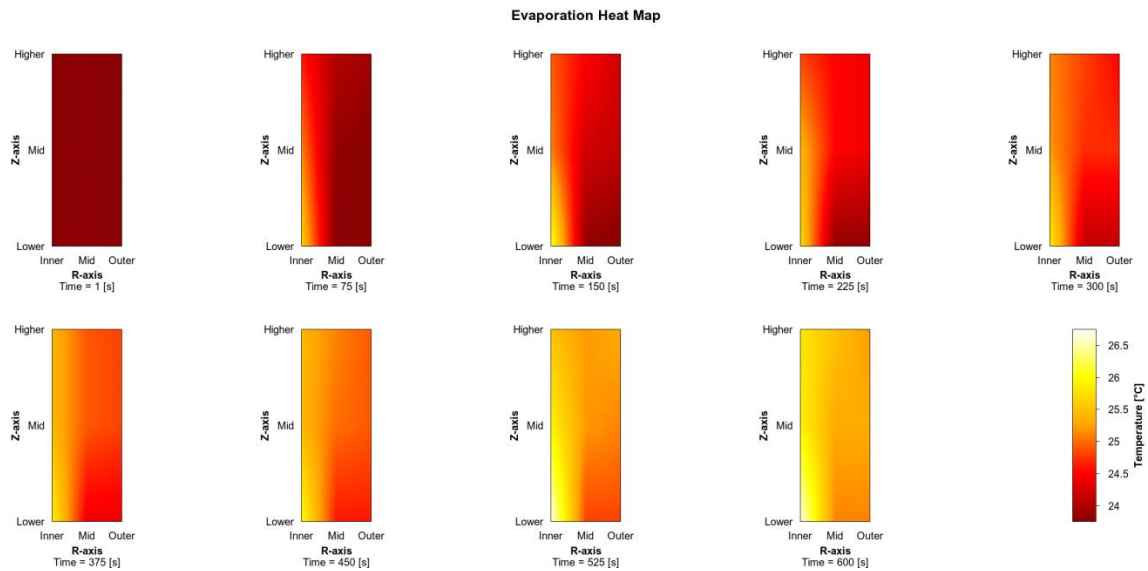**Fig. 3** Convection current in the R-Z plane during the first minutes: Experimental data (190 dm³ system)
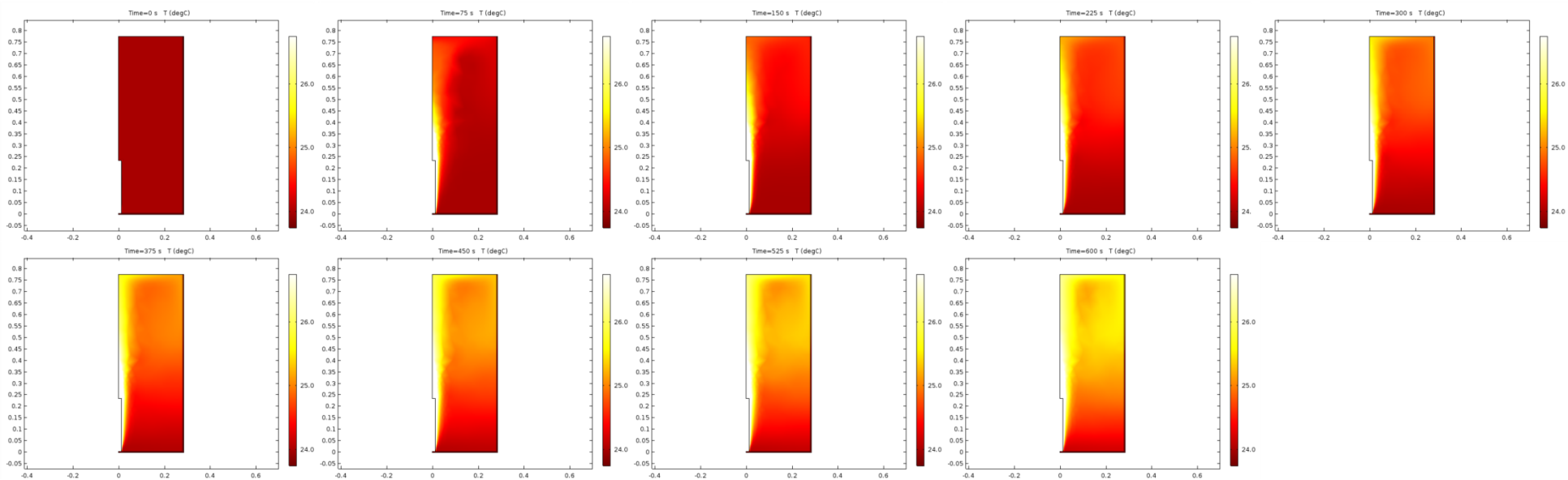

Fig. 4 Convection current in the R-Z plane during the first minutes: CFD simulation using COMSOL (190 dm³ system)
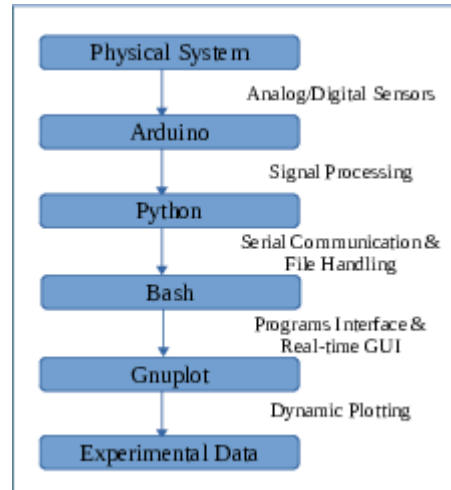
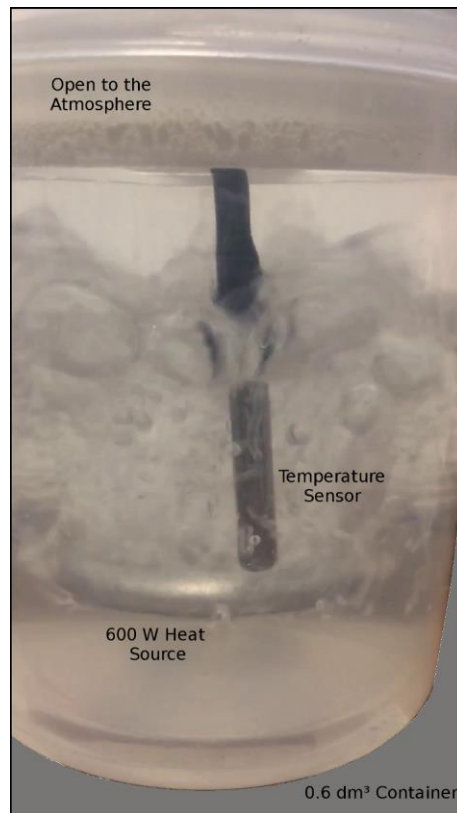**Fig. 5** Data acquisition flow diagram using open source software

Fig 6. Evaporation experiment second configuration with 0.6 dm³ (Behavior shown at 1000 [kW/m³])

2.2 Zero-order model

The evaporation rate in water bodies with or without localized heat sources competes with different mechanisms that supply and dissipate energy from the system. In addition, geometric characteristics and other factors such as dissolved particles or additives to the fluid can have a significant influence in the evaporation rate by modifying the system configuration. If these water bodies are used as thermal reservoirs, the material properties of the container or surfaces that transfer heat, and the medium that receives the evaporation flow may also play dominant roles on the accuracy of the calculated reservoir conditions. Regarding the heat source, in the most general case it is accompanied by mass sources. Nevertheless, this analysis is limited only to those cases where they are negligible.

Given all the parameters that can interact in the process, an approach using a zero-order model was selected with the assumption that every mechanism involved can be grouped in a linear or exponential contribution as indicated in equation (1). Moreover, this approach is assumed reasonable as long as the balance is not disturbed by water loss associated with evaporation. When that disturbance occurs a second phase with a new non-linear behavior will appear until the bulk temperature of the system reaches saturation.

$$T(t) = A + Bt - C_1 e^{-Dt} \quad (1)$$

2.3 Reduced Order Model

Fundamental heat transfer mechanisms associated with evaporation in water bodies may or may not highly depend on fluids motion, as is the case of convection, boiling and evaporation, but unlike conduction or radiation. Based on this and the fact that only a few degrees difference in the body water temperatures were observed during thousands of seconds in the experimental runs, a ROM (Reduced Order Model) with point-geometry and global thermodynamic parameters was considered as a first approximation to the heat and mass transfers taking place. Here, internal convection is treated as the energy deposited in the liquid, corresponding to left-hand side of equation (2), while the right-hand side considers the

energy system inlets and outlets, that is, the mechanisms that supply and dissipate energy, with or without loss of mass.

$$m(t)C_p\frac{dT}{dt} = \dot{Q}_{\text{in}} - \dot{Q}_r - \dot{Q}_c^W - \dot{Q}_c^P - \dot{Q}_v - \dot{Q}_b \quad (2)$$

Finch and Hall [4] mention that the dominant meteorological factor that controls the annual evaporation in bodies of water with a diameter greater than 10 m is usually the radiation received by the surface. On the other hand, the main mechanism that supplies energy in systems of smaller-scale is generally an external source to the liquid, such as a heat exchanger or an electric resistance heater submerged in it. For this study, the system input $(\dot{Q}_{\text{in}})$ corresponds to the submerged electrical resistance controlled by the data acquisition system.

As to the dissipation mechanisms, in large-scale systems radiation can also be constituted as the dominant factor, and therefore models like that of *Penman* [5] analyze the net surface radiation, although more accurate predictions tend to depend on the estimation of the available energy. Such estimation requires accounting for the variation in storage capacity or energy transferred to or from the water body by other sources. That refinement can be done directly or indirectly, as in the model of *Edinger et al.* [6] with the introduction of an equilibrium temperature and the corresponding time constant.

In general, if the liquid temperature is known, the radiation $(\dot{Q}_r)$ emitted by a surface can be estimated using Stefan-Boltzmann's law as shown in equation (3), where J*acobson* [7] treats the emissivity of water approximately as one.

$$\dot{Q}_r = \epsilon^W \sigma \left[T(t)^4 - T_{amb}{}^4 \right] \quad (3)$$

For small-scale systems, external convection with the surrounding air and conduction through the floor of the container are generally more relevant. Therefore, a global description of the

geometric configuration must be incorporated into the ROM, as in the case of water surface convection $\left(\dot{Q}_c^W\right)$, governed by Newton's law of cooling and described in equation (4).

$$\dot{Q}_c^W = h_c^W A_{Surf}(T - T_{amb}) \quad (4)$$

Conduction at the body boundaries can be thought of as a special type of convection where the heat transfer coefficient is a function of the conductivity and thickness of the material. As consequence, it is lumped with the heat dissipated by convection through the plastic $\left(\dot{Q}_c^P\right)$ in the ROM, using the floor area as a weighting factor detailed in equation (5).

$$\dot{Q}_c^P = h_c^P \left(P_{wall} \left[H_0 - \frac{m_L(t)}{\rho(t) \times A_{surf}} \right] + A_{Floor} \right) [T_w - T_{amb}] \quad (5)$$

The mass loss effect is also coupled in equation (5) through the dynamic heat transfer lateral area that depends on the water level. The external temperature of the wall is a function of the temperature in the ROM, derived from experimental measurements and corresponding to equation (6).

$$T_w = T - \Delta T_{w_{MAX}} \times \left[1 - e^{\frac{T_{amb} - T}{\lambda_w}} \right] \quad (6)$$

The energy dissipated by evaporation loss can be approximated by a model with the structure proposed by *Singh and Xu* [8] as shown in equation (7), where the pressure deficit is the dominant factor for monthly or greater time spans. In contrast, for phenomena of shorter duration, the impact of the wind function or forced convection must be accounted for in the ROM model.

$$\dot{Q}_v^G = \rho A \times f(u)g(P)h(T) \times L \quad (7)$$

For this study, the evaporation model was reduced to the convective-like function $\left(\dot{Q}_v\right)$ described in equation (8) assuming the pressure difference that governs the evaporation

mass rate can be decomposed to its temperature dependence if the water body and air temperatures near the surface are known.

$$\dot{Q}_v = h_v A_{surf}(T - T_{air}) \quad (8)$$

The wind function is implemented through a weighting relation detailed in equation (9) that modifies the air temperature above the water surface to account for the local increase in the temperature primarily due to mass transfer.

$$T_{air} = \eta T + (1 - \eta)T_{amb} \quad (9)$$

Finally, the ROM also includes the mass loss associated with boiling around the localized heat source. According to *Bergman et al.* [9] boiling "occurs when the temperature of the surface T_s exceeds the saturation temperature T_{sat} corresponding to the liquid pressure", and in general is characterized by a complex dynamic.

However, if the external heat source displays a constant behavior and its power is such that the generation of bubbles is instantaneous, the energy dissipated by the bubbles $(\dot{Q}_b)$ can be estimated by comparison with the response of the system assuming a sigmoid function that accounts for the bubble collapse during the trajectory to the water-air surface, as shown in equation (10).

$$\dot{Q}_b(t) = \frac{\dot{Q}_{b_{MAX}}}{2} \times \left[1 + \frac{1 - e^{\frac{t_b - t}{\tau_b}}}{1 + e^{\frac{t_b - t}{\tau_b}}}\right] \quad (10)$$

Table 1 contains all the parameters used during the ROM and CFD implementations. The parameters not related to the geometry were estimated from dimensionless analysis or derived from experimental data.

Table 1 Reduced order model parameters

Parameter	Value	Units
$\dot{Q}_{in}$	1600	W
ϵ	1	-
h_c^{W} [a]	43	$\dfrac{W}{m^2 \times K}$
D_{surf}	0.56	m
T_{amb}	18.7	°C
h_c^{P} [a]	8	$\dfrac{W}{m^2 \times K}$
$\Delta T_{w_{MAX}}$ [b]	17.9	°C
λ_w [b]	21	°C
h_v	77	$\dfrac{W}{m^2 \times K}$
η	$\dfrac{1}{2}$	-
$\dot{Q}_{b_{MAX}}$	285.6	W
t_b	43,340	s
τ_b	10,550	s

[a] Dimensionless analysis

[b] Experimental data

2.4 Computational Fluid Dynamics model

The COMSOL[1] Multiphysics® CFD modeling software was used to replicate the 190 dm³ group of experiments carried out to investigate the relative impact of different boundary conditions above the water-air surface on the system response. Figure 7 shows the lid temperature distribution for the case with a fin submerged in the water body at approximately 3 hours into the experiment.
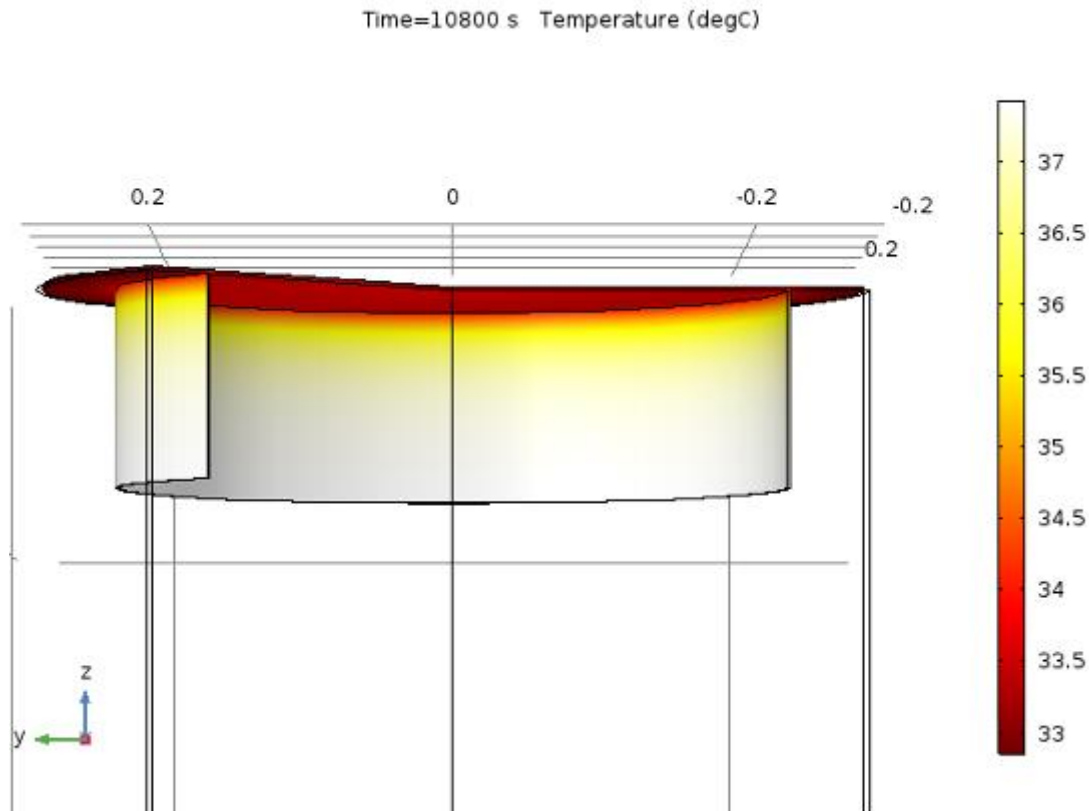
Time=10800 s   Temperature (degC)

Fig. 7 Lid temperature distribution for the case with a submerged fin

The CFD code employed finite-element methods to solve for the velocity field, pressure and the water, wall and lid temperatures with the density as coupling variable (Fig. 4). The three-dimensional geometry was simplified assuming azimuthal symmetry. The mesh is mainly composed of triangular elements with 5 rectangular layers around the walls and after a mesh refinement study the results displayed low sensitivity to the grid.

---

[1] COMSOL was selected due to its large library of physics models, as well as its integrated and friendly interface.

The heat transfer coefficients in the solid interfaces correspond to the values obtained in the dimensionless analysis used in the ROM. Turbulence was simulated using the $k - \omega$ model [10] due to its applicability to wall-bounded flows [11] and the phase change dynamics were implemented through boundary conditions derived from the ROM.

A 10-hour period was simulated for each boundary condition, with a relative tolerance of 1% in the time dependent solver. The results agreed well with the observations, presenting a relative error of less than 3% in all cases.[2]

3. Results and discussion

Heat and mass transfer parameters involved in this study were estimated through the computation of separate dimensionless numbers using a quasi-steady approximation with special emphasis at the beginning of the experiment and at the temperature reached once a close balance between the heat source and the body water energy losses was observed. Figure 8 summarizes the results obtained from this analysis indicating the dominance of convection over conduction.
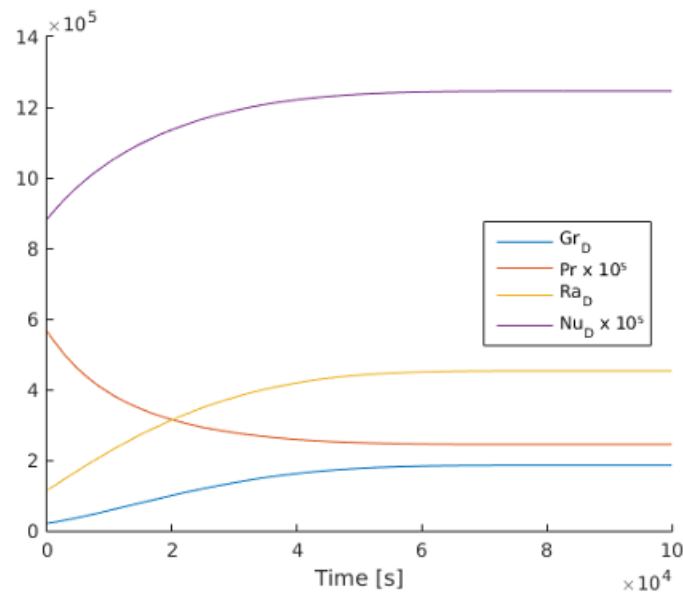

Fig. 8 Dimensionless numbers evolution between initial conditions and power-balance temperature (190 dm³ system)

---

[2] $\frac{T_{CFD} - T_{Exp}}{T_{Exp}} \times 100$

3.1 Boundary conditions impact

Figure 9 shows the experimental water body temperature evolution for different boundary conditions above the surface-air interface at an ambient pressure of 77 kPa. In particular, by including a lid to limit fluid losses due to evaporation, it can be noticed that the benefit of retaining more liquid in the system does not overcome the temperature increase associated with a rise in the local pressure. This observation holds whether or not the lid has direct contact with the liquid through a submerged fin[3], or if its external face is cooled down by forced convection[4].
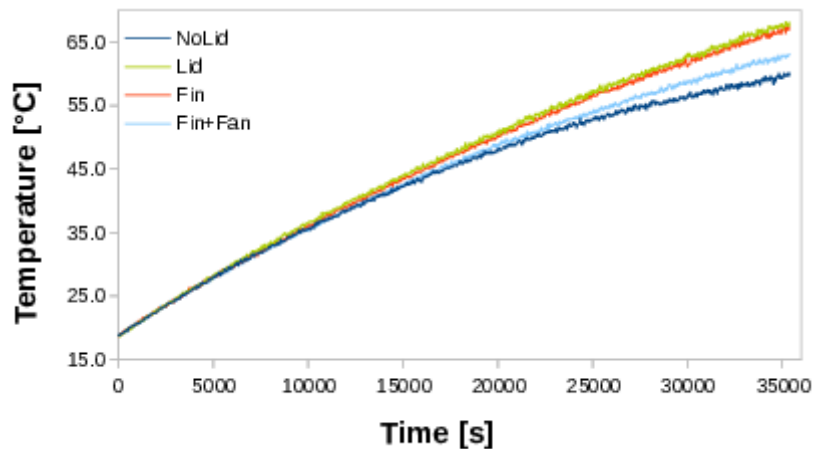

Fig. 9 Temperature evolution for different boundary conditions at 77 kPa (190 dm³ system)

The impact of conduction on the fin is limited because condensation at the inner face of the lid is the dominant heat transfer mechanism. A set of passive external fins could potentially help to cool the system but the setup with an active fan appears to be the limiting case. Air saturation above the water reservoir has a severe impact on the evaporation rate, if the air gets saturated the reservoir temperature will increase because the evaporation mass flow is inhibited.

There is an initial period of time during which the body water heat-up when natural convection is the dominant mechanism of energy transport from the heat source to the surroundings. Naturally, the initial temperature affects the global response due to the energy already stored

---

[3] The fin had a height of 13.5 cm, a thickness of 1 mm, and was located 5 cm away from the plastic wall, approximately.
[4] Fan velocity around 5 m/s

in the system, therefore this period can be estimated by studying the interval starting at the moment with the lowest common temperature until the observed system response remains virtually identical for all cases. For this configuration, that period of time corresponded to 3.3 hours approximately and a temperature less than 38.2 °C.

On the other hand, Figure 10 displays the impact of the ambient pressure in the experiments without the lid, where the relative humidity and the ambient temperature become as relevant as the water body surface temperature in regulating the evaporation rate. The case with the lid at 77 kPa is included in the figure as a reference. The experimental system and zero-order model responses after 24 hours for the setup without the lid at a pressure of 85 kPa can be observed in Figure 11, where the error bars are plotted assuming the experimental data as reference.
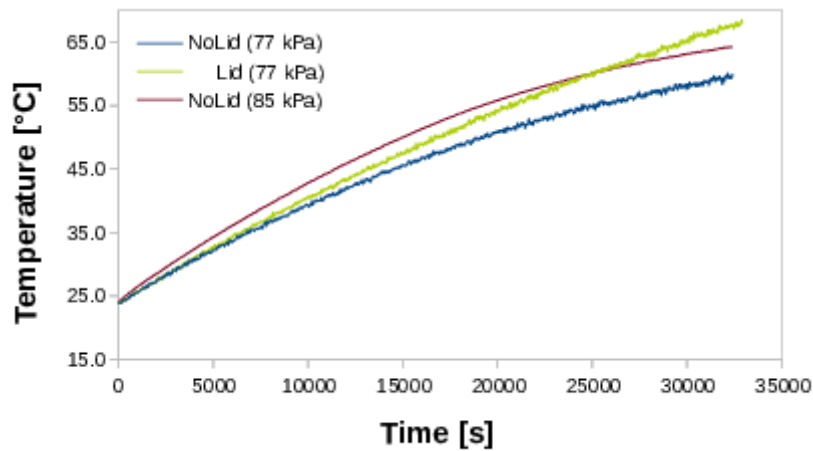

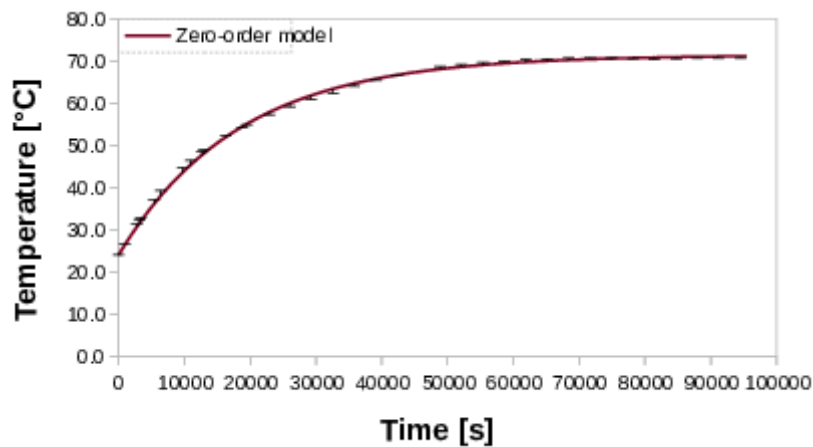**Fig. 10** Temperature evolution at different ambient pressure (190 dm³ system)

Fig. 11 Zero-order model temperature response after 24 hours with error bars from experimental data (190 dm³ system, $r^2 = 0.99677$)

When the exponential behavior is dominant, it can be inferred based on the experimental data that coefficient A is associated with the water body temperature at balance, coefficients B and D correspond to the permanent and transient responses of the system respectively, and coefficient C_1 is determined by the initial conditions of the experiment. All of them were derived without segmenting or adding weights to the experimental data using a code written in Matlab, whose output was verified analytically for the case with ideal conduction at constant wall temperature.

Table 2 contains the values of those coefficients for different boundary conditions tested with the first configuration, where $\frac{1}{D}$ corresponds to the time constant of the transient response τ and coefficient C_1 represents the total variation in water body temperature from the initial conditions to the temperature at balance. Meanwhile, coefficient B is related to the energy stored in the system and coefficient A acts as a function of the ambient pressure and supplied power. The impact of the lid can be noticed in the rather large values of coefficient B with respect to coefficient D, implying the exponential behavior is no longer dominant. In general, the long-term reservoir temperature response depends on the heat source intensity as well as on the ambient pressure. It is observed that a 10% power increase in this study results in a similar response to a 10 kPa pressure increase, corroborating that the evolution is a function of the stored energy, as the setups with lid clearly confirm.

Table 2 Zero-order model coefficients for different boundary conditions at 77 kPa (190 dm³ system)

Pressure [kPa]	Average Power [W]	Duration [h]	T_0 [°C]	Lid Presence	A [°C]	B [°C/s]	C_1 [°C]	D [1/s]	r^2[5]
77	1569	26.5	24.0	No	65.7	0.000002	41.7	0.000051	0.9955
85	1600	26.5	24.0	No	71.2	0.000002	47.2	0.000055	0.9975
85	1532	65.1	24.0	No	70.2	0.000011	46.2	0.000057	0.9953
77	1559	10.0	18.7	Yes	72.1	0.000421	53.4	0.000029	0.9998
77	1839	10.0	18.7	Yes	92.3	0.000451	73.6	0.000024	0.9994

---

[5] The coefficient r^2 is derived using Matlab "Goodness-of-Fit" statistics.

Figure 12 shows the evaporation rate measured through the liquid surface depth, depicting the essentially immediate loss of water that occurs in the system, as well as its corresponding second-order polynomial fit. The gap in the frequency of the error bars is due to time periods without recorded measurements.

3.2 Power density as a figure of merit

The experimental data from the second configuration was obtained using the power density to differentiate evaporation with local boiling where bubbles remain mostly attached to the heated surface, from non-local boiling, where the phase change implies an abrupt separation and chaotic movement of the bubbles. Table 3 describes the transition of these stages in relation to the power density.

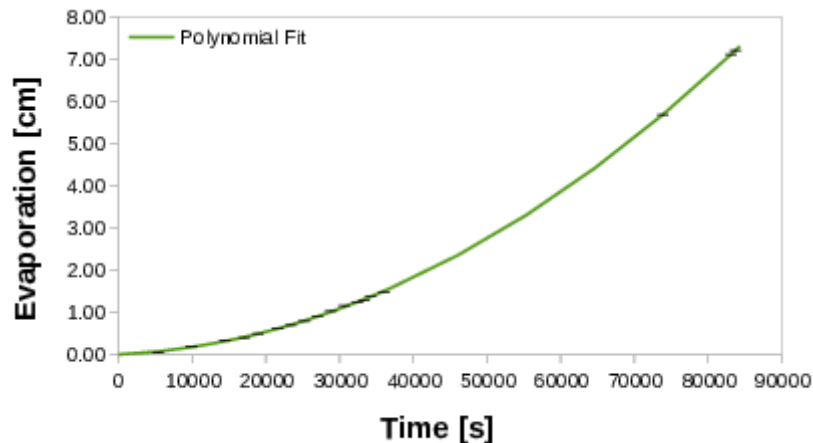**Fig. 12** Evaporation rate after 24 hours with error bars from experimental data (190 dm³ system)

A summary of the behavior of the small-scale system under different power densities is shown in Table 4. The form of the model for these cases was assumed identical to that of the larger-scale experiments to estimate the conditions in which such approach no longer represented the dynamic of the system.

Table 3 Characteristics of evaporation transition between local and non-local boiling (0.6 dm³ system)

Power Density [kW/m³]	Temperature [°C]	Power Balance	Bubble Formation[a]	Bubble Size[b]	Bubble Dettachment[c]	Bubble Movement[d]
1+	31.9	Yes	None	-	-	-
10	56.6	Yes	Minimal	Small	Slow	-
100	54.7	No	Minimal	Small	Slow	-
100	77.8	No	Constant	Small	Frequent	Steady
100	87.5	No	Constant	Medium	Frequent	Steady
100	90.0	Yes	Constant	Large	Frequent	Turbulent
1000	70.4	No	Constant	Small	Frequent	Steady
1000	92.2	Yes	Constant	Large	Fast	Turbulent

[a]Minimal refers to sporadic nucleation of bubbles over the heated surface, constant indicates no apparent change in the frequency of formation during the complete test. Bubbles collapse before reaching the surface at 1+ kW/m^3 as well as at the other power densities when the system temperature is low with respect to the equilibrium temperature.

[b]Medium denotes ¼ of the heated surface diameter, small and large indicate sizes above and below ¼ of the heated surface diameter

[c]Frequent corresponds to ¼ of a second approximately, slow and fast indicate detachment periods above and below ¼ of a second.

[d]Steady and turbulent refer to the apparent motion of bubbles after they have been detached from the heated surface.

Table 4 Zero-order model coefficients for different power densities (0.6 dm³ system)

Power Density[a] [kW/m³]	T_0 [°C]	A [°C]	B [°C/s]	C_1 [°C]	D [1/s]	r^2
2.2	16.5	31.4	0.000003	14.9	0.000243	0.845
10.6	16.3	55.1	0.000039	38.8	0.000271	0.994
107.4	15.1	92.1	0.000001	77.0	0.001188	0.985
1023.4	18.2	92.3	0.000001	74.1	0.005686	0.946

[a]Actual values shown

Coefficient A bears a good relationship with the temperature at balance for this configuration. For a power density equal or greater than 100 kW/m³, coefficient B denotes that the system evolves too rapidly for the linear component to be relevant, having the ambient temperature a similar effect for values around 1 kW/m³. Additionally, above 100 kW/m³ coefficient D tends to predict the temperature reached at balance more slowly than in the actual large-scale system, but shows good agreement with the response of the system in the other cases.

It can be seen from Figure 13 that the coefficient of determination (r^2) associated with the output of the zero-order model correlates well with the previous assessment and can be used to estimate a region where the transition in evaporation between local and non-local boiling occurs under this approach. Figure 14 shows the effect of ambient temperature in the oscillating temperature at balance for the case with a power density close[6] to 1 kW/m³. In contrast, the temperature at balance for 10 kW/m³ presents a clear linear component contribution.

On the other hand, for power densities larger than 100 kW/m³ and due to bubble mass transport the non-local boiling has a dominant effect in the heat transfer to the surface over natural convection. This effect brings proportionally closer the bulk temperature of the system to the saturation temperature.

---

[6] Actual power density was around 2.2 kW/m³.

Furthermore, three distinct regions can be identified in each curve: A flat region where convection is the main mechanism of heat transport, a transition region characterized by a competition between sensible and latent heat, and a power-balance region where evaporation becomes the prevailing mechanism of heat transfer. The duration of the first region, the slope of the second region and the temperature behavior during the third region can be all related to the power density. For example, in the lowest power density case, the convection is the dominant mechanism for around 1000 s, taking approximately 10000 s after that to reach its balance temperature, with an oscillating temperature of around 32 °C.

For power densities of different order of magnitude, the time to reach power-balance and the difference between the balance and saturation temperatures appear to have a linear relationship. As shown in Figure 15, increasing the power density reduces the time the system has to dissipate energy, except for the case with the lowest power density, where the influence of the ambient temperature is more significant.
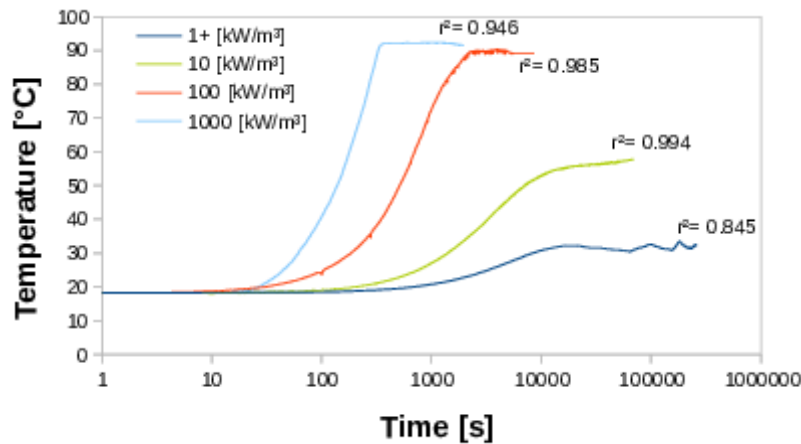

Fig. 13 Temperature evolution for different power densities at 77 kPa (0.6 dm³ system)
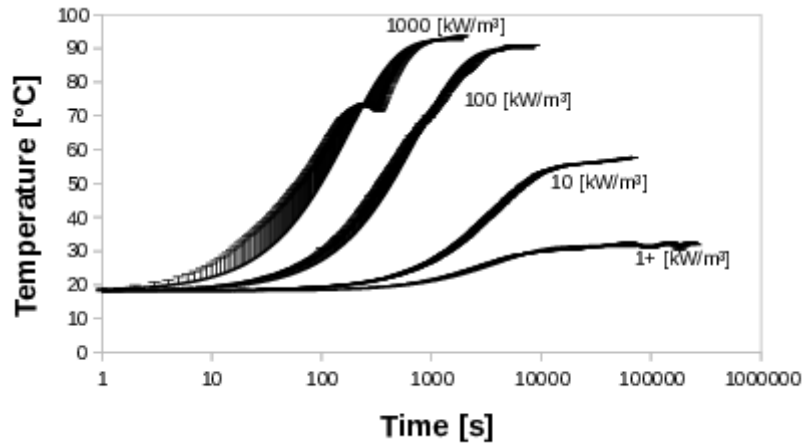
Fig. 14 Zero-order model temperature response for different power densities with error bars from experimental data (0.6 dm³ system)
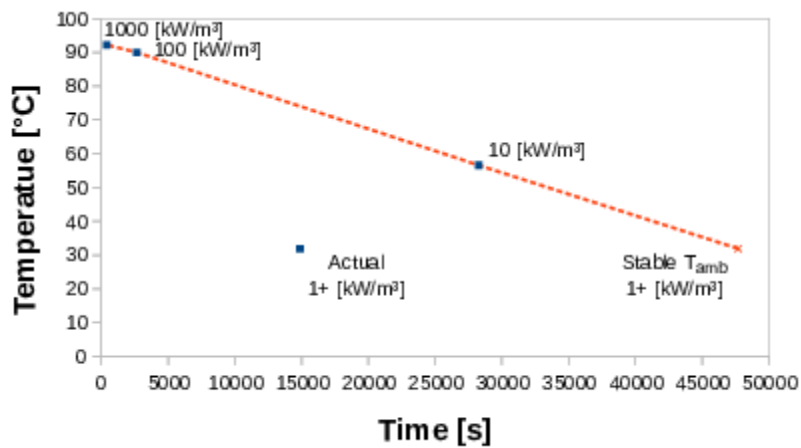
Fig. 15 Power-balance temperature for different power densities. The stable T_{amb} value corresponds to the trend prediction without the influence of ambient temperature (0.6 dm³ system)

In accordance with Figure 16, the evaporation mass flow exhibits a non-linear behavior that tends to increase as the water volume loss takes place and evaporation becomes the main dissipation mechanism, where the transition time is determined by the power density in the system

Fig. 16 Evaporation rate after 24 hours for different power densities. The second degree polynomial trend is shown in dash lines (0.6 dm³ system)

Finally, for the range studied in the second configuration, Figure 17 shows that on a logarithmic scale the time required to evaporate half the volume in the system holds a linear relationship with the heat source power density.
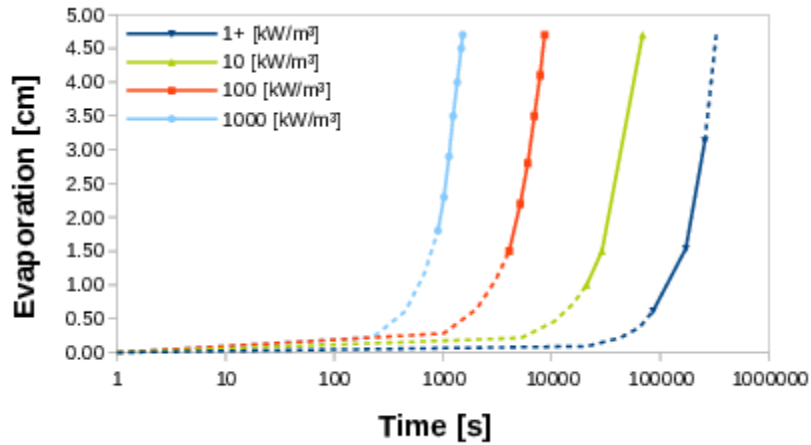

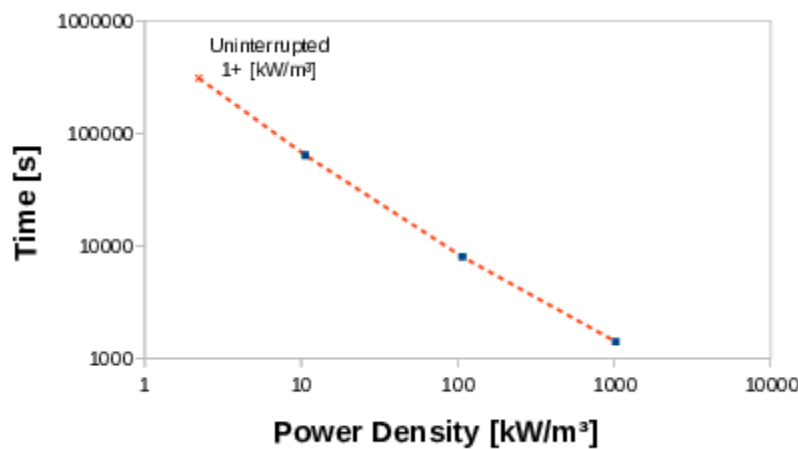**Fig. 17** Time to evaporate 50% of the initial volume for different power densities. The uninterrupted value corresponds to the trend prediction for an experiment lasting more than 72 hours (0.6 dm³ system)

3.3 Scaling effects

Another important factor that has to be considered to determine the methodology to be used in the analysis is the time-space scale of the problem. The test without lid at a pressure of 77

kPa from the first configuration was compared to the case with the closest power density from the second configuration to get insight into the impact of the scale in the response of the system.

Table 5 shows how the temperature increase to reach power balance is roughly the same in both cases, even though the initial temperature was different. The time constant is an order of magnitude faster in the small-scale configuration and the linear component is significant an order of magnitude earlier, although non-dominant in both cases.

The surface to volume ratio for the small-scale configuration in this study is one order of magnitude higher than in the large-scale configuration as detailed in Table 6, resulting in an evaporation rate three times as fast in comparison with the large-scale system.

Table 5 Zero-order model coefficients comparison between cases with similar power density

Experiment Configuration	Power Density [kW/m³]	V_0 [dm³]	T_0 [°C]	Duration [h]	A [°C]	B [°C/s]	C_1 [°C]	D [1/s]	T [s]
1	8.3	190	24.0	26.5	65.7	0.000002	41.7	0.000051	19608
2	10.6	0.6	16.3	19.3	55.1	0.000039	38.8	0.000271	3690
2 to 1 Ratio	1.28	0.003	-	-	0.84	19.5	0.93	5.31	0.19

Table 6 Time response comparison between cases with similar power density

Experiment Configuration	Power Density [kW/m³]	Volume [dm³]	S/V [m]	50% Height [cm]	Time to 50% Height [h]
1	8.3	190	1.3	38.5	71.7
2	10.6	0.6	11.9	4.2	23.3
2 to 1 Ratio	1.3	0.003	9.2	0.1	0.3

3.4 ROM results

A modified Jakob number (Ja*) described in equation (11) is proposed to analyze the phase change behavior associated with boiling near the heat source. The modification consisted of (1) including the liquid and vapor density in the numerator and denominator respectively, and (2) changing the temperature difference from the usual wall superheat to the difference between the average and equilibrium temperatures. That is, the reference temperature for Ja* is set to the equilibrium temperature, where the fraction of supplied power used to increase the water body temperature is minimal due to the balance with the dissipation mechanisms.

$$Ja^*_{Properties} = \frac{\rho_L c_P (T_{eq} - T)}{\rho_V L} \quad (11)$$

The Ja* derived from the ROM is estimated analogously to equation (11) as the ratio of sensible heat to boiling heat dissipated by the bubbles during the whole simulation as shown in equation (12). The ROM boiling heat transfer appears to be underestimated during the initial part of the simulation, but in general shows good agreement for a ROM as can be seen in Figure 18, specifically, they share the same order of magnitude and the same general behavior.

$$Ja^*_{ROM} = \frac{m(t) C_p \frac{dT}{dt}}{\dot{Q}_b} \quad (12)$$
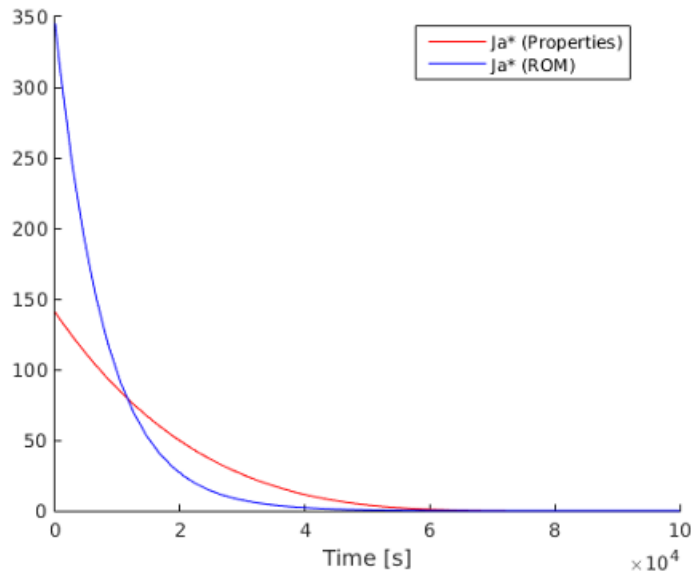

Fig. 18 Sensible heat vs. Boiling heat: Proposed Jakob number derived from thermal properties and simulation results

The water body temperature evolution recorded in the experiment and the values predicted by the ROM are depicted in Figure 19, including the measurements for the wall temperature and the estimated air temperature above the water surface. The ROM temperature (Yellow) is in good agreement with the 77kPa experimental data (Continuous, purple), and it is bounded by the behavior of the more detailed 85kPa experimental data (Dotted, purple). Similarly, Figure 20 contains the ROM prediction regarding mass loss distribution between evaporative flow (Blue) and bubbles that reach the water-air surface (Red), as well as its sum (Yellow) compared with the experimental data (Purple).

Figure 21 shows the evolution of the different heat dissipation mechanisms under the ROM. The dominant mechanisms correspond to the two interactions in the water-air surface (Convection in dark blue and evaporation in light blue, collectively known as $\dot{Q}_{surf}$). Radiation heat (Red) is the least significant mechanism, although not negligible. The power-balance is reached approximately after 22 hours.

Finally, Figure 22 details the water body long-term response predictions estimated using the ROM, departing from power-balance due to the change in lateral-convection dissipation caused by water level reduction and its runaway effect. The shroud case is derived assuming the heat source has been partially encased to delay the lateral heat transfer $\left(\varDelta T_{w_{MAX}} = 22.9[°C]\right)$. The Two Phase Closed Thermosyphon (TPCT) case approximates the addition of a secondary system sized to fully condense and return the extracted mass ($m_L = 0$), preventing the departure from power-balance. Finally, the fan case assumes the air temperature above the surface is closer to the ambient temperature by means of forced convection ($\eta = \frac{1}{4}$).
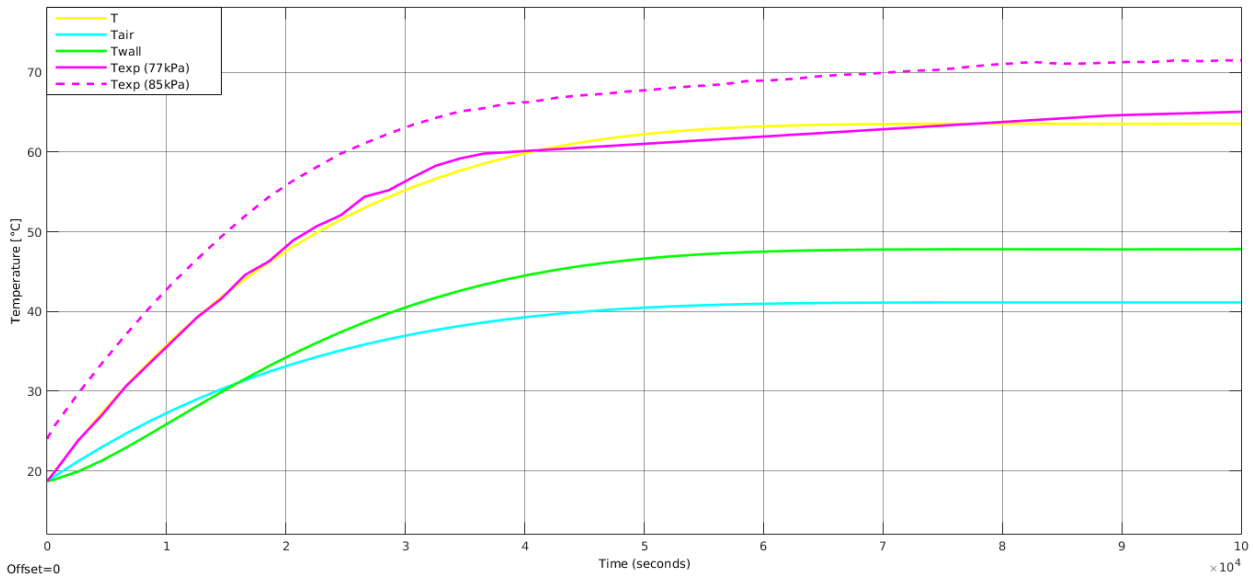
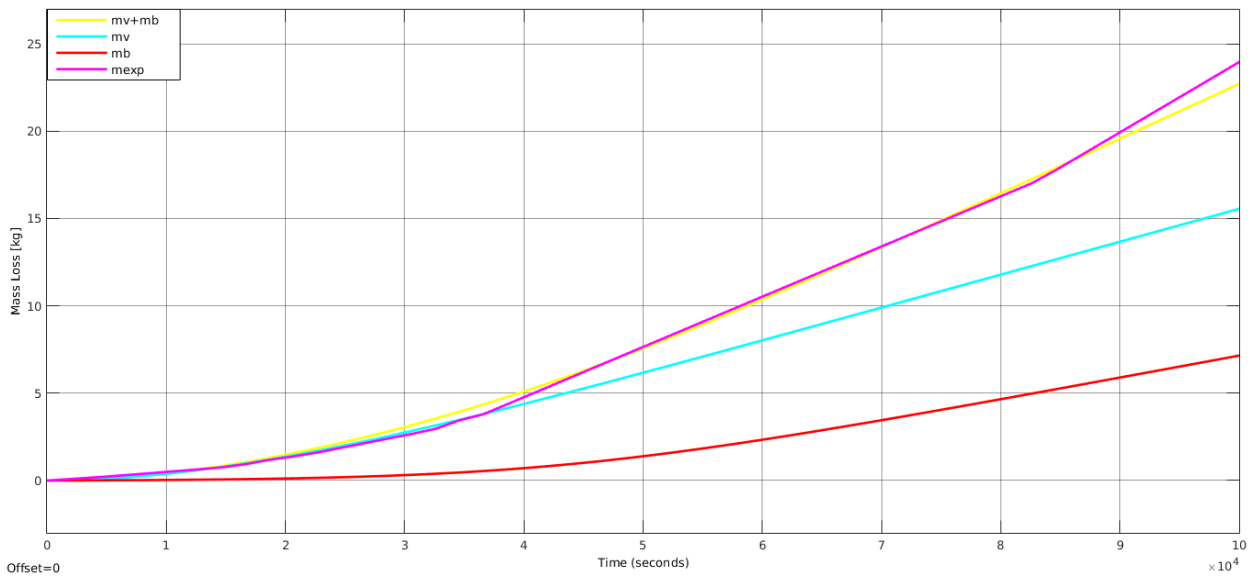**Fig. 19** Temperature evolution under the Reduced Order Model

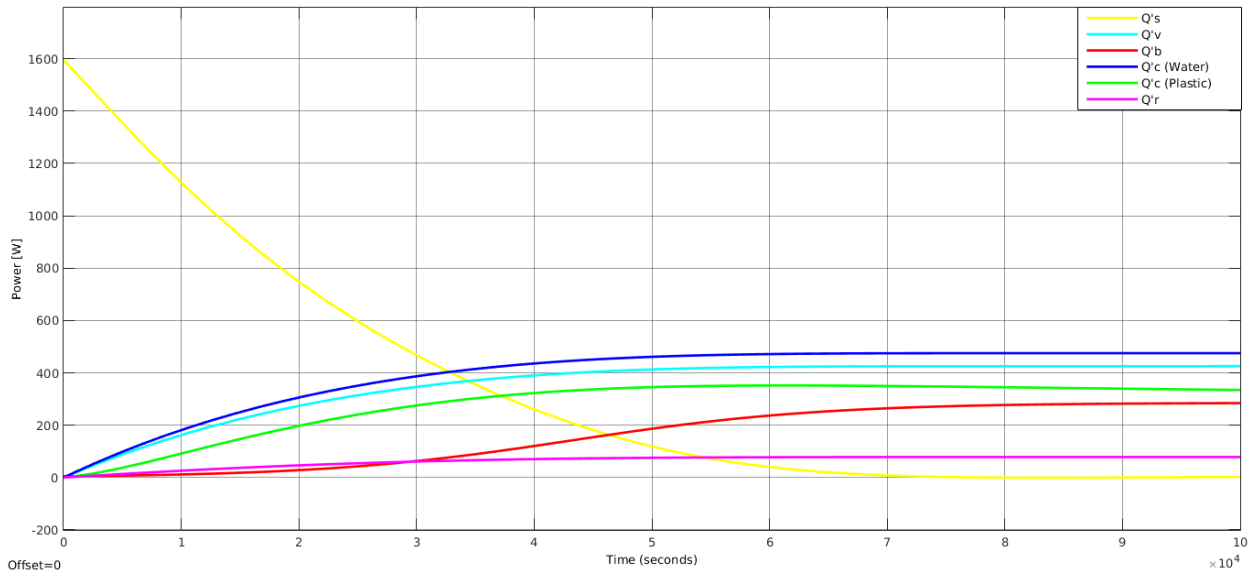**Fig. 20** Mass loss under the Reduced Order Model

Fig. 21 Heat dissipation mechanisms under the Reduced Order Model
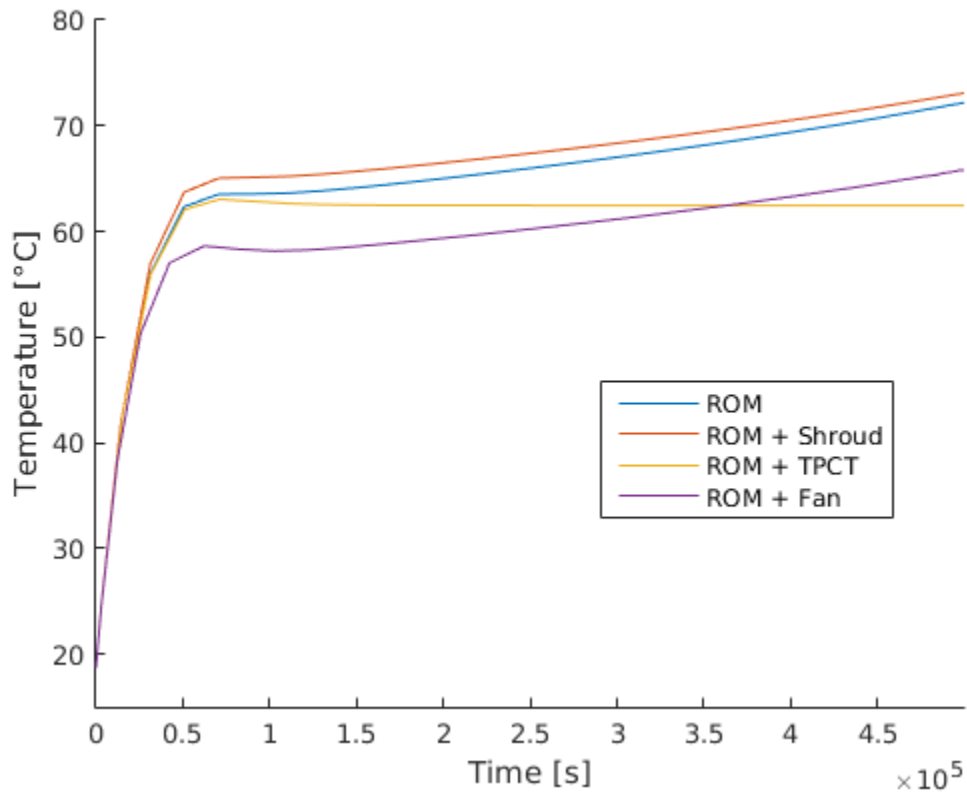
Fig. 22 Long-term response predictions estimated using the Reduced Order Model

3.5 CFD model results

Figure 23 displays the temperature evolution comparison between the CFD simulations results and the data recorded in the different boundary conditions. The largest discrepancy corresponds to a 1.7°C difference in the case without lid and is a consequence of the approximations to the phase change dynamics in the boundary conditions.
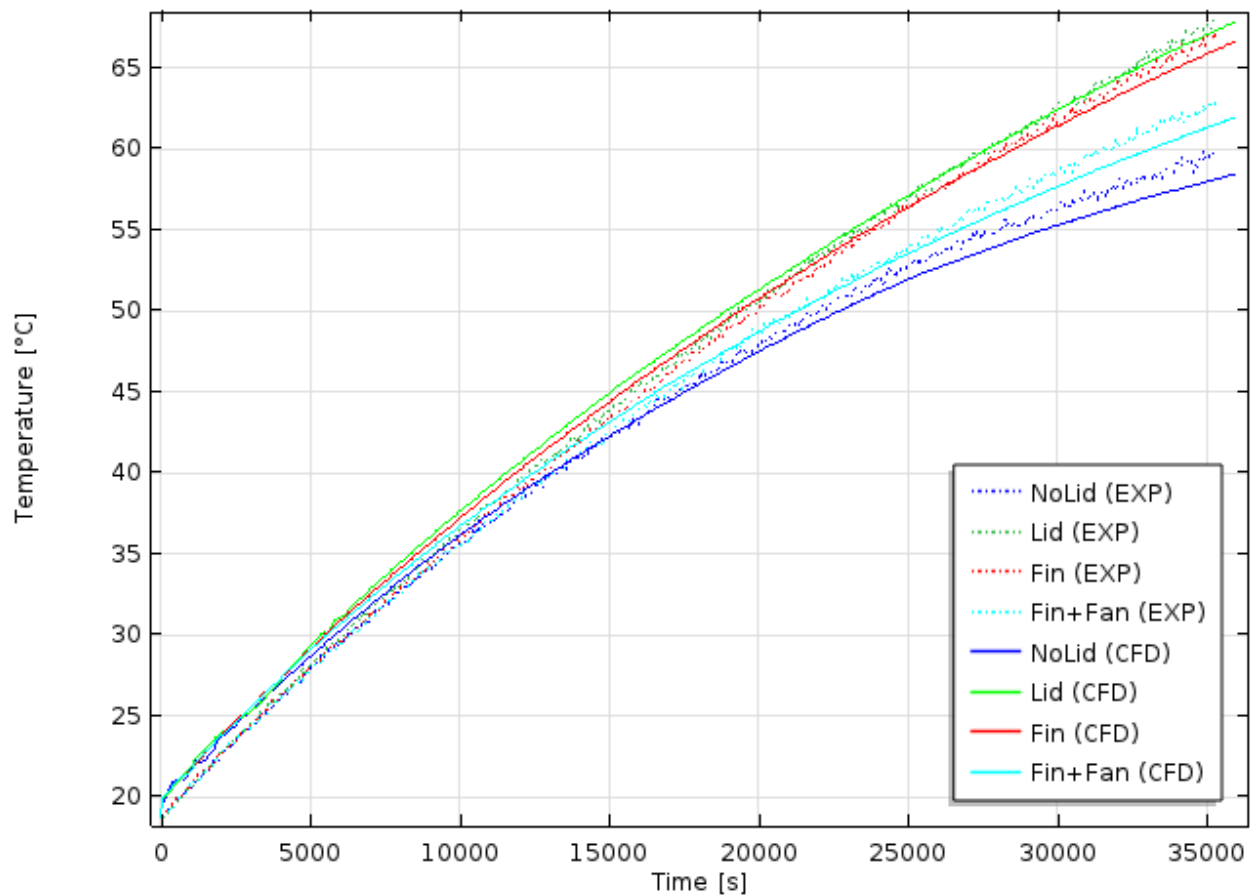
Fig. 23 CFD Temperature evolution derived for the different boundary conditions

The transient response of heat mechanisms and its relative impact as derived from the CFD simulations for the different boundary conditions can be seen in Figure 24. The heat transfer through the plastic surfaces and the radiated heat remain mostly the same, although the lateral convection in the plastic is approximately 4 times more significant. The sensible heat deposited in the water gets reduced to less than half when comparing the cases with and

without lid[7]. The reduction in sensible heat is compensated by an increase in the water-air surface convection in the cases with lid, and ultimately by the evaporation rate in the case without it. The dissipation by bubble escape is only considered in the case without lid and is minimal during the 10-hour period.
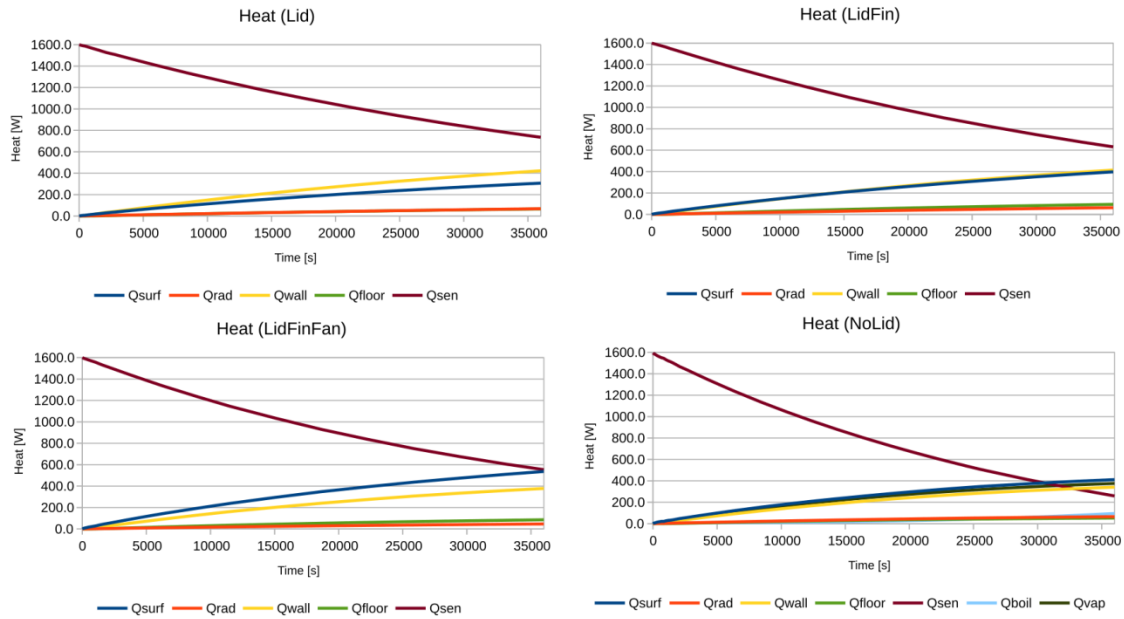
Fig. 24 CFD Heat mechanisms relative impact for different boundary conditions. Values derived from the simulations considering the integrated average temperature in each domain

The heat transfers through the water-air surface with or without mass transport are the most significant dissipation mechanisms throughout the present study. When these mechanisms are inhibited by adding a lid, the temperature of the system increases its tendency to reach saturation, but even in that case the system temperature stabilizes below saturation due the low power density.

---

[7] . The seal formed by the lid was tight enough that a piece of tape used to cover a small penetration inflated during the experiment, indicating an increase in both temperature and pressure. The lid CFD simulation assumed ideal conditions with no escape of mass.

4. Conclusions

The following aspects were studied in this paper: The long-term spatial and temporal transient response of a system involving boiling and evaporation as well as conduction and convection due to a localized heat source in terms of power dissipation and mass loss using a combined ROM-CFD analysis. The distinction between water evaporation and boiling using the power density as a figure of merit to determine the most appropriate approach to quantify mass and energy long-term evolution in heated water bodies.

The major findings are: (1) The heat transfers through the water-air surface with or without mass transport are the most significant dissipation mechanisms throughout the present study. When these mechanisms are inhibited by adding a lid, the temperature of the system increases its tendency to reach saturation, but even in that case the system temperature stabilizes below saturation due the low power density. (2) When the heat source power density is less than 100 kW/m³, a simple evaporation analysis becomes a viable approach to approximate the long-term behavior of the large-scale system.

References

[1]   Çengel, Y. A., and M. A. Boles (2006), Properties of pure substances, in Thermodynamics: An Engineering Approach, p. 151, McGraw-Hill Higher Education, New York.

[2]   Thacker, B. H., S. W. Doebling, F. M. Hemez, M. C. Anderson, J. E. Pepin, and E. A. Rodriguez (2004), Concepts of model verification and validation, Rep. LA-14167-MS, Los Alamos National Laboratory.

[3]   Wong, K. V., and O. De Leon (2010), Applications of nanofluids: current and future, Adv. Mech. Eng., 2, 519659.

[4]   Finch, J. W., and R. L. Hall (2001), Estimation of Open Water Evaporation, Rep. W6-043/TR, Environment Agency.

[5]   Penman, H. L. (1948), Natural evaporation from open water, bare soil and grass, Proc. R. Soc. Lond. A Math. Phys. Eng. Sci., 193(1032), 120–145.

[6]   Edinger, J. E., D. W. Duttweiler, and J. C. Geyer (1968), The response of water temperatures to meteorological conditions, Water Resour. Res., 4(5), 1137–1143.

[7]   Jacobson, M. Z. (2005), Radiative energy transfer, in Fundamentals of atmospheric modeling, p. 277, Cambridge university press, New York.

[8]   Singh, V. P., and C. Y. Xu (1997), Evaluation and generalization of 13 mass-transfer equations for determining free water evaporation, Hydrol. Process., 11(3), 311–323.

[9]   Bergman, T. L., A. S. Lavine, F. P. Incropera, and D. P. DeWitt (2011), Boiling and condensation, in Fundamentals of heat and mass transfer, p. 655, John Wiley & Sons, New Jersey.

[10]   Wilcox, D. C. (1998), Turbulence modeling for CFD, 2nd ed., DCW industries, Inc., La cañada, CA.

[11]   Dewan, A. (2011), k–ε and other two equations models, in Tackling turbulent flows in engineering, p. 69, Springer Science & Business Media, Heidelberg.

TRAC-U – CFD Analysis of Nanofluids in Heated Water Bodies

Abstract

In the present study the nanofluids impact in heat transfer mechanisms due to convection and conduction effects, as well as during phase change is analyzed through the implementation of TiO_2 and Al_2O_3 nanofluids properties in CFD and a thermal-hydraulic two phase 1D-transient model based on TRAC-BF1 routines. TRAC-U is introduced as a systematic and ongoing attempt to incorporate new developments into TRAC-BF1. The analysis uses the optimized model developed for chapter 1 and a model developed in TRAC-U. It is found that the impact on the system depends on the dominant mechanism of heat transfer. The density appears to be the most significant parameter in both models considering the five properties modified in the implementation of nanofluids.

1. Introduction

The objective of this paper is to study the effect of nanofluids on the thermal response of heated water bodies using TRAC-U assisted by Computational Fluid Dynamics (CFD). The importance of nanofluids lies in their ability to enhance the thermal conductivity, convective heat transfer and critical flux of a system without the erosion and sedimentation associated with microparticles.

Nanofluids can be simply defined as colloidal dispersions of nanoscopic particles (1-100 [nm]) in a base fluid. Any liquid such as oils and alcohols can be used as base fluid, but water and ethylene glycol are the most common due to their properties as refrigerant and antifreeze respectively. Some common materials used as nanoparticles due to their already high conductivity are naturally metals (Ag, Cu, Au), and certain carbon allotropes (Nanotubes, graphene, diamond), but also metal oxides (Al_2O_3, TiO_2, CuO) due to their impact on surface wettability (Coursey and Kim [1]).

Yu and Xie [2] reviewed different preparation methods and found that the production of nanoparticles as dry powders followed by a dispersion step into a base fluid like sonication[8] is the most widely used method. However, the stability (Sedimentation and clustering) of the nanofluid is problematic giving rise to the use of surfactants[9] or the development of one step methods where the dispersion occurs simultaneously with the production of the nanoparticles.

Fang et al. [3] reviewed a large number of experimental investigations involving nanofluids spanning more than a decade and found that there is still a conflict in the results related to boiling heat transfer, with 53.6% of the cases reporting enhancement, 39.3% deterioration and 7.1% no effect. The maximum values reported[10] were a deterioration of 40% and an enhancement of 200%. In the case of the critical heat flux (CHF) there is a clear trend with 90.5% of the cases reporting enhancement, 7.9% deterioration and 1.6% no effect. The maximum values reported were a deterioration of 75% and an enhancement of 245%.

---

[8] Ultrasonic agitation aimed to prevent the mixture from acting as a suspension.
[9] Surface active agents that reduce the surface tension.
[10] The maximum values correspond to different solid phases of Al_2O_3.

Ciloglu and Bolukbasi [4] analyzed different parameters related to nanofluid pool boiling and reached the conclusion that there is an optimum value in nanoparticles concentration where the both heat transfer coefficient (HTC) and CHF improve, after which the CHF remains stable but the HTC deteriorates. At low concentrations they found an increment in nucleation sites with the nanofluids superior thermal conductivity being the dominant effect. However, at high concentrations a reversal occurs with a blockage of nucleation cavities and the dominant effect being the formation of an additional thermal resistance caused by a layer of nanoparticles deposited over the heated surface during boiling.

Forrest et al. [5] applied different nanoparticle coatings to heat transfer surfaces whose description ranges from hydrophobic to superhydrophilic and found that in all cases there is an enhancement in CHF, concluding that a low contact angle[11] yields a higher CHF. The previous nanoparticle coating instead of the deposition during boiling suggests that the microscopic characteristics of the surface are the main reason behind the increment in CHF. However, some experimental investigations have also considered the nanoparticles impact on the heat of vaporization of the base fluid, reporting increase (Chen et al. [6], Ameen et al. [7]), reduction (Tso and Chao [8], Bhuiyan et al. [9]) and both effects (Lee et al. [10], Lee et al. [11]) depending on the type, size and concentration of nanoparticles.

In both cases the enhancement mechanism seems to be strongly related to the interaction between the nanoparticles dispersed in the fluid and those deposited over the surface. This interaction explains the CHF enhancement dependency on transient duration (Sharma et al. [6]). The boiling heat transfer deterioration under subcooled conditions (Taylor and Phelan [7]), and the presence of a liquid microlayer underneath the bubbles or the improved bubble emission frequency in hydrophilic surfaces (Phan et al. [8]), help to illustrate the complexity of such interaction[12].

---

[11] High wettability.

[12] Other factors to consider in the interaction include the presence of surfactants and the operating pressure, as well as other dynamic parameters in the case of nanofluid flow boiling.

2. Methods

2.1 Nanofluid properties

Chandrasekar et al. [12] showed that the theoretical mixing approximation[13] for nanofluid density underestimates the value when compared with hydrometer as well as volume and mass measurements, resulting in a conservative approach for refrigerants.

$$\rho_{[nf]} = \phi\rho_{[np]} + (1 - \phi)\rho_{[bf]} \quad (1)$$

Zhou and Ni [13] found experimentally that nanofluid specific heat capacity is reduced with larger volumetric concentrations and at the same time departs greatly from the theoretical mixing approximation. However, they concluded there was good agreement with the values predicted by a model derived assuming thermal equilibrium between the nanoparticles and the base fluid.

$$C_{p[nf]} = \frac{\phi[\rho C_p]_{[np]} + (1 - \phi)[\rho C_p]_{[bf]}}{\rho_{[nf]}} \quad (2)$$

Lee et al. [14] measured a significant increase in the nanofluid viscosity and thermal conductivity that was directly proportional to the volumetric concentration. In the case of viscosity, the most general approach corresponds to the model introduced by Brinkman [15]

$$\mu_{[nf]} = \frac{\mu_{[bf]}}{(1 - \phi)^{2.5}} \quad (3)$$

which extends to larger concentrations the formula derived by Einstein[14] for spherical shaped particles assuming an ideal particle packing fraction. Chen et al. [16] demonstrated that a more detailed approach requires taking into account the shape of the nanoparticles, its size and the size of the agglomerates that may occur at higher concentrations.

---

[13] The volume concentration is used to calculate a weighted average in a binary mixture.

[14] Applying binomial approximation, Einstein's model is within a 10% tolerance for concentrations up to 16.5%.

An analogous analysis for the thermal conductivity can be made about the model adapted from that proposed by Maxwell [17] for the electrical resistance in a low concentration compound medium, that also results in a conservative approach since it does not incorporate the Brownian[15] motion effect.

$$\frac{k_{[nf]}}{k_{[bf]}} = \frac{k_{[np]} + 2k_{[bf]} + 2\phi(k_{[np]} - k_{[bf]})}{k_{[np]} + 2k_{[bf]} - 2\phi(k_{[np]} - k_{[bf]})} (4)$$

These four properties are sufficient to characterize the nanofluid behavior during forced convection, however for natural circulation it also required to model the thermal expansion since it allows to estimate the density variations in the base fluid[16]. Elhajjar et al. [18] verified that the theoretical mixing approximation does not lead to a good approximation of the thermal expansion, suggesting instead the use of a thermal equilibrium model.

$$\beta_{p[nf]} = \frac{\phi[\rho\beta]_{[np]} + (1-\phi)[\rho\beta]_{[bf]}}{\rho_{[nf]}} (5)$$

The surface tension is directly related to surface wettability[17]. However, due to the minimal variation reported with the addition of nanoparticles (Das et al. [19], Zhu et al. [20]), the nanofluid surface tension was assumed identical to that of the base fluid.

---

[15] Temperature can have a significant effect on the Brownian motion effect, but the nanoscopic size of the particles constitutes the dominant factor.

[16] In this context the Reynolds number is also replaced by the Grashof number as part of the process to evaluate the competition between advection and diffusion, as well as to derive the heat transfer coefficient.

[17] Through Young's equation.

Table 1 Thermal properties of water and different metal oxide nanoparticles

Property	Unit	Water	ZnO	TiO$_2$	Al$_2$O$_3$	CuO
T	K	298	300	293-300	300	293-300
ρ	$\dfrac{kg}{m^3}$	997	5600	4230	3600	6000
C_p	$\dfrac{J}{kg \times K}$	4181	514	692	765	551
ρC_p	$\dfrac{J}{m^3 \times K}$	4.2×10^6	2.9×10^6	2.9×10^6	2.8×10^6	3.3×10^6
k	$\dfrac{W}{m \times K}$	0.6	13	8.4	36	33
β	$\dfrac{1}{K}$	2.6×10^{-4}	4.3×10^{-6}	9.0×10^{-6}	8.5×10^{-6}	4.3×10^{-6}
μ	$Pa \times s$	8.9×10^{-4}	—	—	—	—
D_p	nm	—	25-80	25-145	25-145	25-80
Reference	—	[21]	[22], [23], [24]	[25], [26]	[22], [23], [26]	[24], [25]

Metal oxides (Table 1) can have a significant thermal conductivity when compared to water and their density helps offset their low heat capacity. Titanium and aluminum oxides[18] were selected as nanoparticles for the present analysis considering the high thermal conductivity range they cover.

Figures 1 through 5 show the impact on the base fluid properties of different fraction of nanoparticles for the metal oxides enlisted in Table 1. At low concentrations (Fig. 1-5), the density, the specific heat capacity, the thermal conductivity, the thermal expansion and the viscosity are quite similar to the base fluid properties. On the other hand, at high concentrations, the properties of the different nanoparticles result in an increase in the density (Fig. 1) and thermal conductivity (Fig. 3), and a reduction in the specific heat capacity (Fig. 2) and thermal expansion (Fig. 4). The viscosity (Fig. 5) is independent of the nanoparticles used, increasing with the concentration.

---

[18] Zinc oxide was previously selected due to its commercial availability and low price at $2.6 per gram (2015 USD), and it may revisited in future experiments when the dispersion step can be fully implemented.

2.2 Computational Fluid Dynamics model

The optimized model developed in COMSOL for chapter 1 was used to implement the nanofluid properties through the definition[19] of new materials with different concentrations of nanoparticles. The model is mainly focused on the nanofluids impact due to convection and conduction effects, treating phase change indirectly as a dissipation mechanism. The nanofluid is assumed to be an ideal homogeneous dispersion, therefore a single phase[20] formulation with temperature dependent properties was selected. The temperature influence in the nanofluid was determined by the base fluid (Table 2).

Table 2 Variation in the thermal properties of water due to temperature
(0-99.6 [°C], 1 [atm])

Property	Unit	Minimum	Maximum	Average	Variation
ρ	$\dfrac{kg}{m^3}$	958.6	1000.0	985.1	4%
C_p	$\dfrac{J}{kg \times K}$	4179	4219	4191	1%
k	$\dfrac{W}{m \times K}$	0.5569	0.6771	0.6334	19%
β	$\dfrac{1}{K}$	-6.776×10^{-5}	7.485×10^{-4}	4.234×10^{-4}	193%
μ	$Pa \times s$	2.828×10^{-4}	1.792×10^{-3}	6.849×10^{-4}	220%
ν	$\dfrac{m^2}{s}$	2.950×10^{-7}	1.792×10^{-6}	6.911×10^{-7}	217%
α	$\dfrac{m^2}{s}$	1.317×10^{-7}	1.676×10^{-7}	1.534×10^{-7}	23%
Pr	—	1.760	13.575	4.690	252%
σ	$\dfrac{N}{m}$	5.899×10^{-2}	7.565×10^{-2}	6.772×10^{-2}	25%

---

[19] Linear interpolation in the temperature range corresponding to the liquid phase at atmospheric presure.
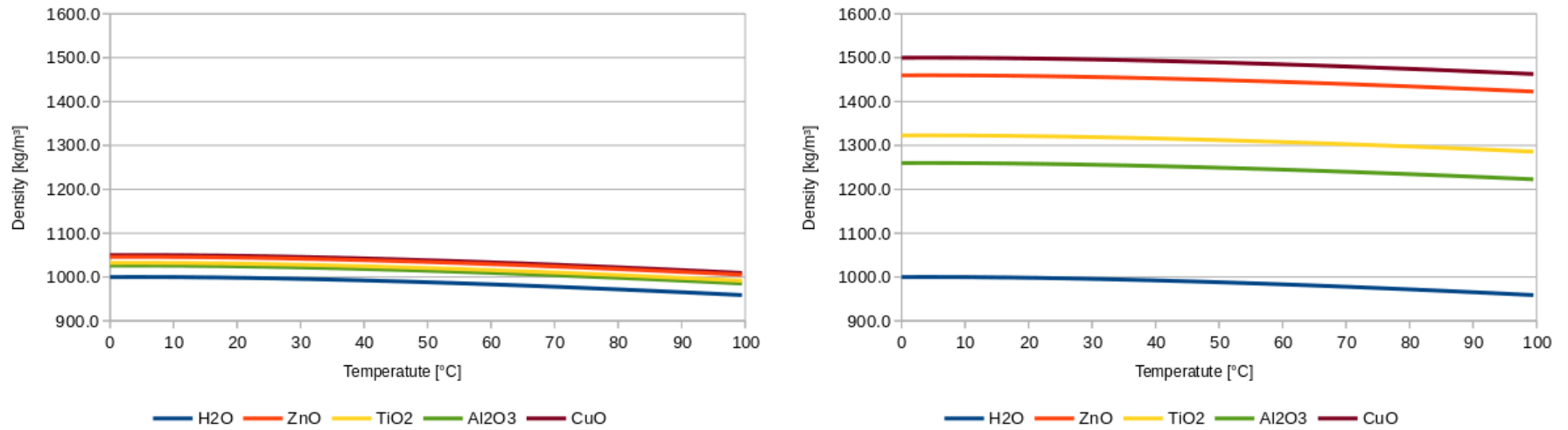[20] No velocity slip between the nanoparticles and the base fluid.

Fig. 1 Nanofluid density with different metal oxides nanoparticles.
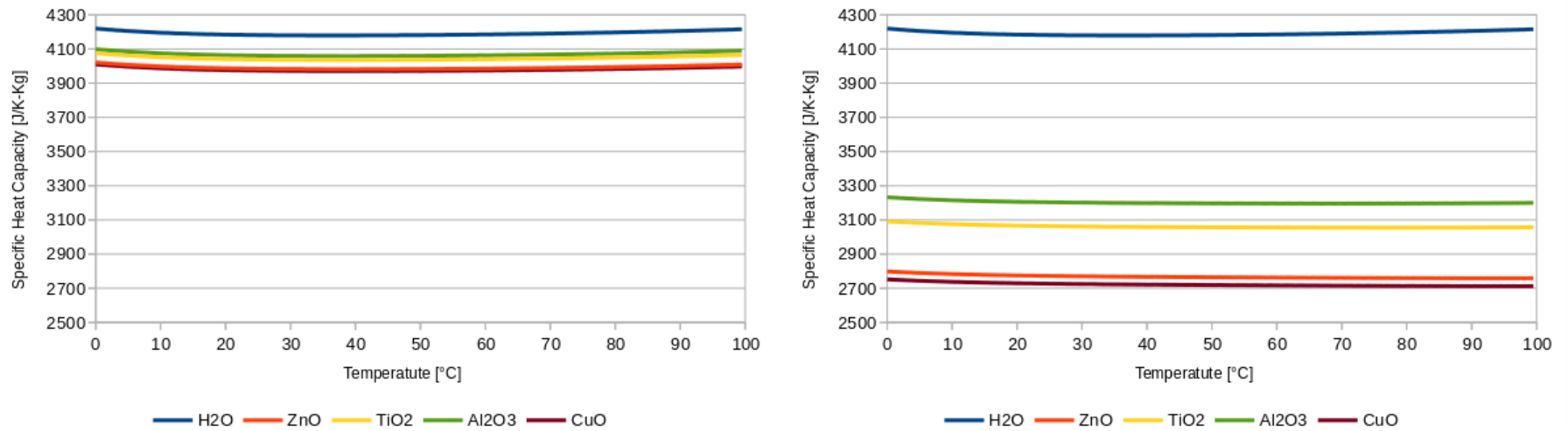Left– 1% volume concentration. Right – 10% volume concentration

Fig. 2 Nanofluid specific heat capacity with different metal oxides nanoparticles.
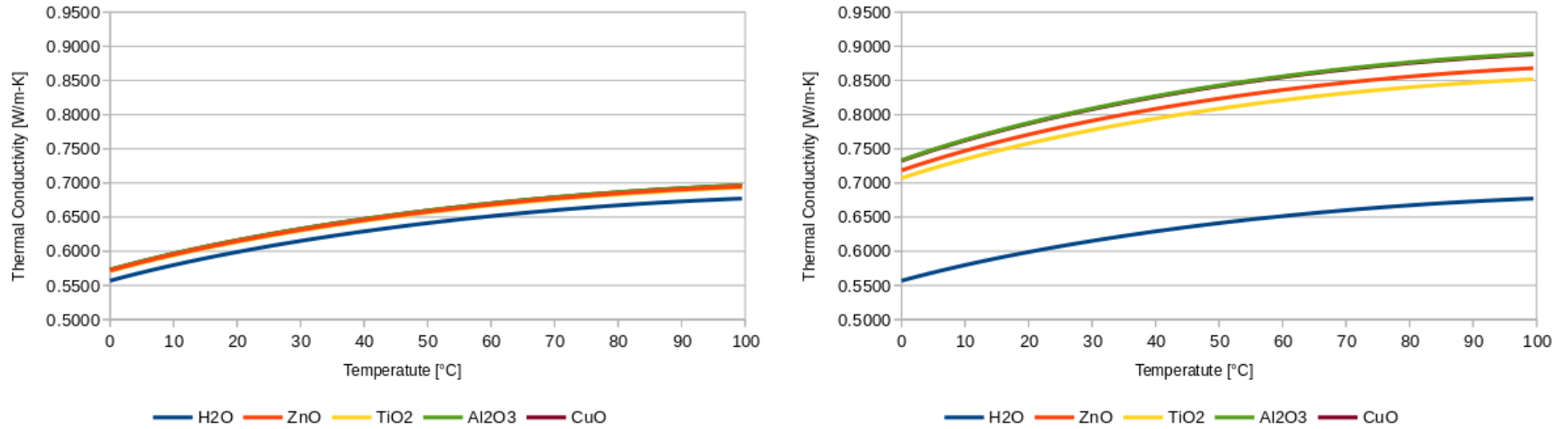Left– 1% volume concentration. Right – 10% volume concentration

Fig. 3 Nanofluid thermal conductivity with different metal oxides nanoparticles.

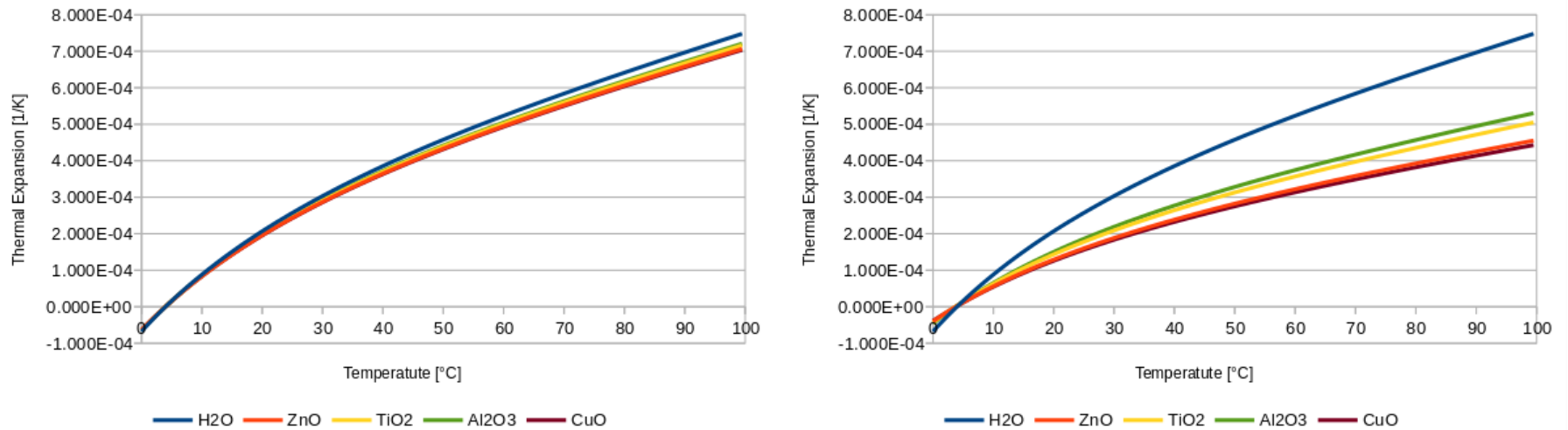Left– 1% volume concentration. Right – 10% volume concentration

Fig. 4 Nanofluid thermal expansion with different metal oxides nanoparticles.

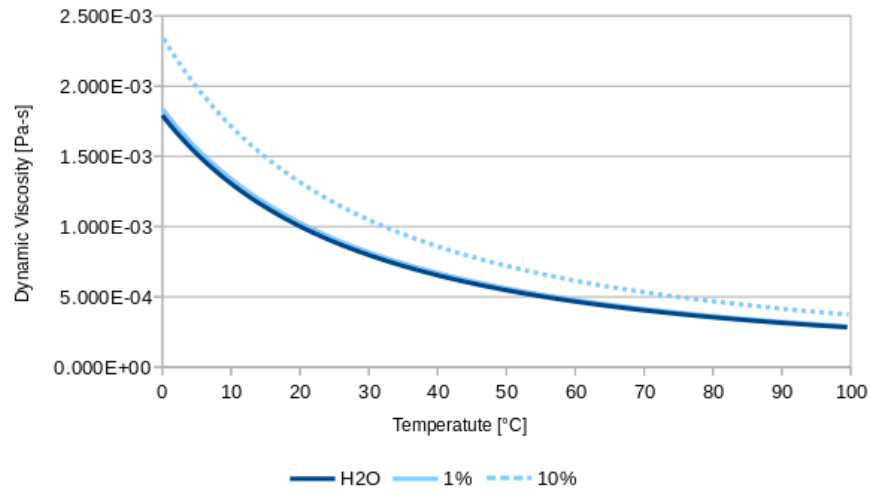Left– 1% volume concentration. Right – 10% volume concentration

Fig. 5 Nanofluid viscosity for different volume concentrations of nanoparticles

The model configuration consisted of a 190 dm³ cylindrical enclosure made of HDPE filled with water-based nanofluids at different concentrations and a 1600 W submerged electrical resistance as external energy source. The model simulated a 10-hour period with an open boundary at the top of the enclosure representing the water-air interface. The results for the reference case without nanoparticles agreed well with the experimental data.

The HTC was derived from the Nusselt number correlation for a non-slender[21] vertical cylinder with free convection flow (Bergman et al. [27])

$$Nu_H = \frac{h \times H}{k} = 0.1 Ra_H^{\frac{1}{3}} (6)$$

where the characteristic length is the height of the power source immersed in the fluid, and the Rayleigh number is calculated as the product of the Grashof and Prandtl numbers evaluated at film temperature.

---

[21] $\frac{D}{L} \geq \frac{35}{Gr_H^{\frac{1}{4}}}$

2.3 TRAC-U model

TRAC-BF1 is a best-estimate thermal-hydraulic code developed by INEL for the analysis of transients and postulated accidents in boiling water reactors (Borkowski et al. [28]), whose MOD2 version dates back to 2000. In the meantime, there have been some developments, particularly those carried out by the US-NRC geared towards the consolidation of other codes safety codes through the use of TRACE[22].

However, these developments do not necessarily invalidate all the capabilities previously demonstrated by TRAC-BF1, but instead establish an opportunity to incorporate them into a new version of the code for academic purposes. TRAC-U is the authors systematic and ongoing attempt to achieve this goal.

The TRAC-BF1 FORTRAN 77 subroutines dedicated to calculate the density, specific heat capacity, thermal conductivity and dynamic viscosity were modified to implement the nanofluid properties for titanium and aluminum oxides at different concentrations. Depending on the phase, TRAC-BF1 estimates the variation of density from the current density or from the ideal gas approximation, and therefore the thermal coefficient of expansion was not modified.

The TRAC-U model is mainly focused on the nanofluids impact during phase change. In accordance with this objective, the model (Table 3) consisted of a single copper solid tube[23] acting as a 2000 W power source immersed in a 74 dm³ pool of water. The pool walls were made of concrete and were allowed to transfer heat to the environment. Analogously to the CFD model, the nanofluid is assumed to be an ideal homogeneous dispersion with temperature dependent properties determined by the base fluid. The reduction in volume as well as the increment in power in comparison with the CFD model were selected to guarantee that at least 1/3 of the total volume was evaporated in the simulated 10-hour period.

---

[22] TRAC/RELAP Advanced Computational Engine.

[23] Channel component.

Table 3 TRAC-U model heat transfer parameters

Parameter	Unit	Value	
$\dot{Q}$	W	2.0×10^{-3}	
D_{Tube}	m	5.08×10^{-2}	
H_{Pool}	m	1.8	
D_{Pool}	m	2.58×10^{-1}	
δ_{Pool}	m	4.23×10^{-2}	
T_0	K	316	
P	Pa	1×10^5	
h_{air}	$\dfrac{W}{m \times K}$	10	
Material	—	**Copper**	**Concrete**
ρ	$\dfrac{kg}{m^3}$	8930	2300
C_p	$\dfrac{J}{kg \times K}$	378.2	1000.0
k	$\dfrac{W}{m \times K}$	399.9	1.7

The HTC was estimated internally by the code from the McAdams [29] natural convection equation:

$$h = 0.13(Gr \times Pr)^{\frac{1}{3}} \times \frac{k}{D_H} \text{(7)}$$

where the characteristic length is the local hydraulic diameter, and the Gr number is calculated from the density variation.

$$Gr = \frac{-g \times (\frac{\partial \rho}{\partial T})_P \times |Tw - T| \times \rho \times D_H^3}{\mu^2} \text{(8)}$$

3. Results and discussion

3.1 CFD model results

The CFD model predicts an enhancement in the convective HTC when water is substituted with a nanofluid as the refrigerant in the system (Fig. 6). The maximum increment corresponds to 11% for TiO_2 and 13% for Al_2O_3. The performance of both nanofluids is quite similar even though the thermal conductivity of Al_2O_3. is more than 4 times that of TiO_2 with an almost identical volumetric heat capacity (ρC_p). This suggests that conduction through the system walls plays a vital role for the optimal use of nanofluids.
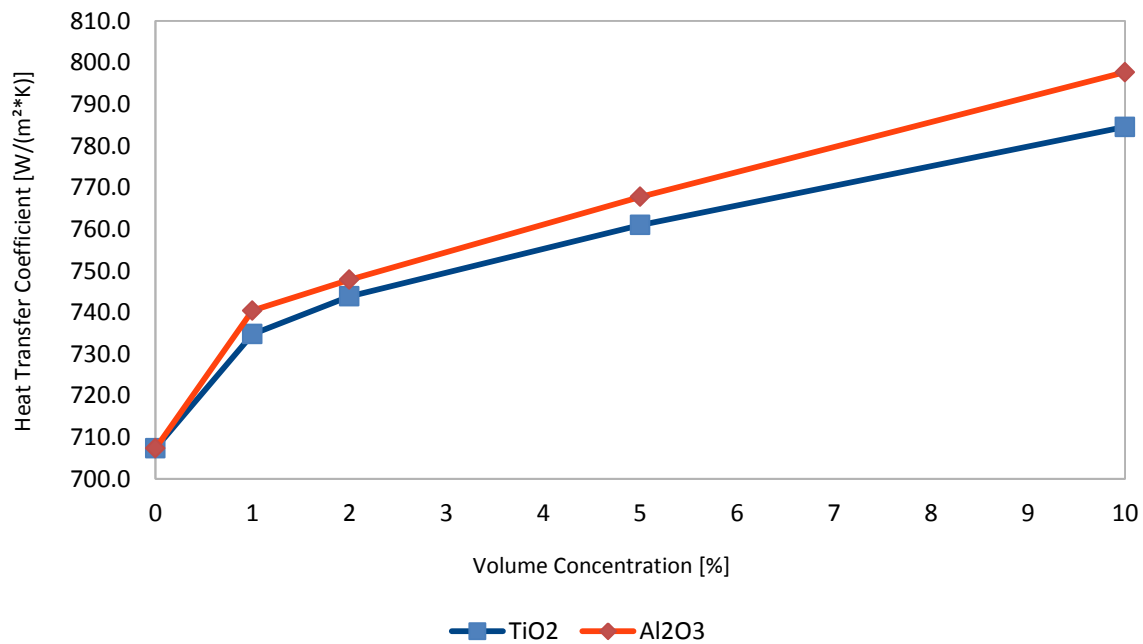

Fig. 6 Heat transfer coefficient for different volume concentrations of nanoparticles (CFD)

Even though the convective HTC was improved, the thermal conductivity was improved even further leading to a reduction in the Nusselt number with an optimal point around a 1% concentration (Fig. 7). The thermal expansion coefficient approximation predicts equivalent variations in density ($\Delta\rho$), while the Prandtl number takes a similar value for both nanofluids. These two effects make the density ($\frac{1}{\rho}$) the dominant factor in the determination of the Raleigh number, explaining the closely related Nusselt number of both nanofluids.

3.2 TRAC-U model results

The thermal properties of the refrigerant are implemented inside the code as enthalpy functions, while the enthalpy is a density function, therefore the density of the nanofluid tends to have a prediction effect in the time response of the system (Fig. 8).

The TRAC-U model does not predict an enhancement in the convective heat transfer when the phase change is considered (Fig. 9), predicting in fact in a reduction. The reduction is independent of the nanofluid used, with a maximum value of 6% for both nanofluids. This similarity is again probably related to the almost identical volumetric heat capacity (ρC_p) of both nanofluids as well as the low thermal conductivity of the walls[24]. The volume concentration of nanoparticles has a limited impact in the system final void fraction with a maximum variation of ± 3% (Fig. 10).

The approach applied in the CFD and TRAC-U models only takes into account the variation in the properties that results from adding nanoparticles to the base fluid, without any effect due to the microscopic characteristics of the surface or the heat of vaporization of the base fluid. The apparent contradiction between the predictions of the two models (The increase in the convective heat transfer derived from the CFD model and the reduction derived from the TRAC-U model), can be explained when the dominant mechanism of heat transfer is considered. The variation in the properties is significant during single phase heat transfer when a combination of convection and conduction is the main mechanism. However, when the phase change is occurring the variation in the properties becomes secondary.

---

[24] In order to approximate the experimental setup used to verify the simulation, the CFD model average thermal conductivity of the walls (HDPE) was $0.26 \frac{W}{m*K}$.

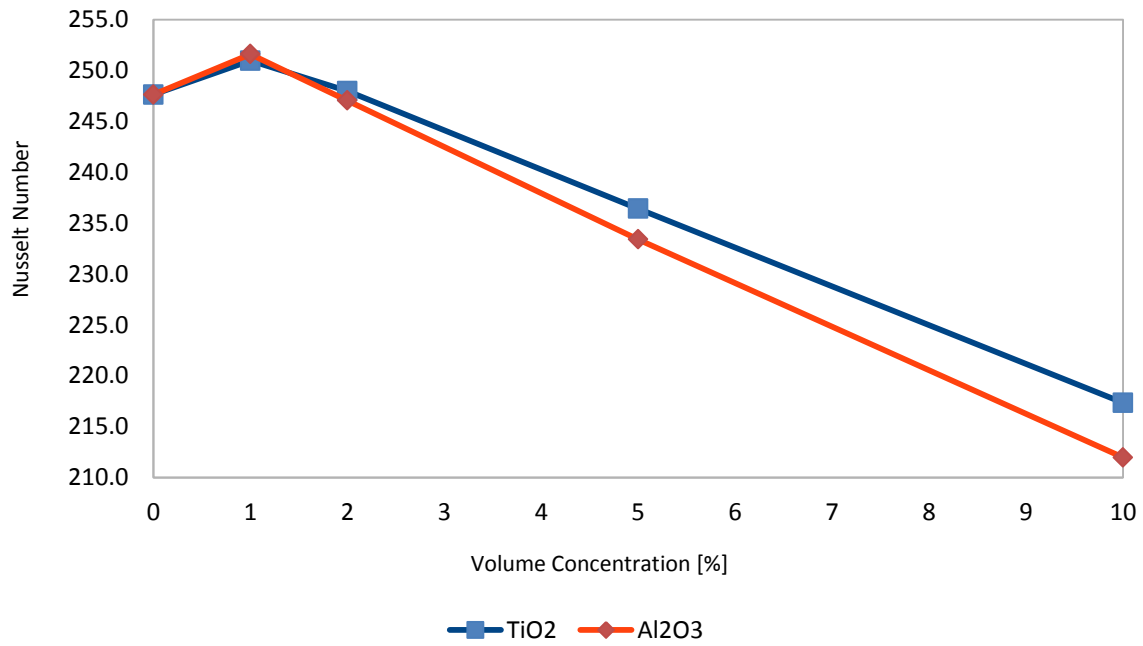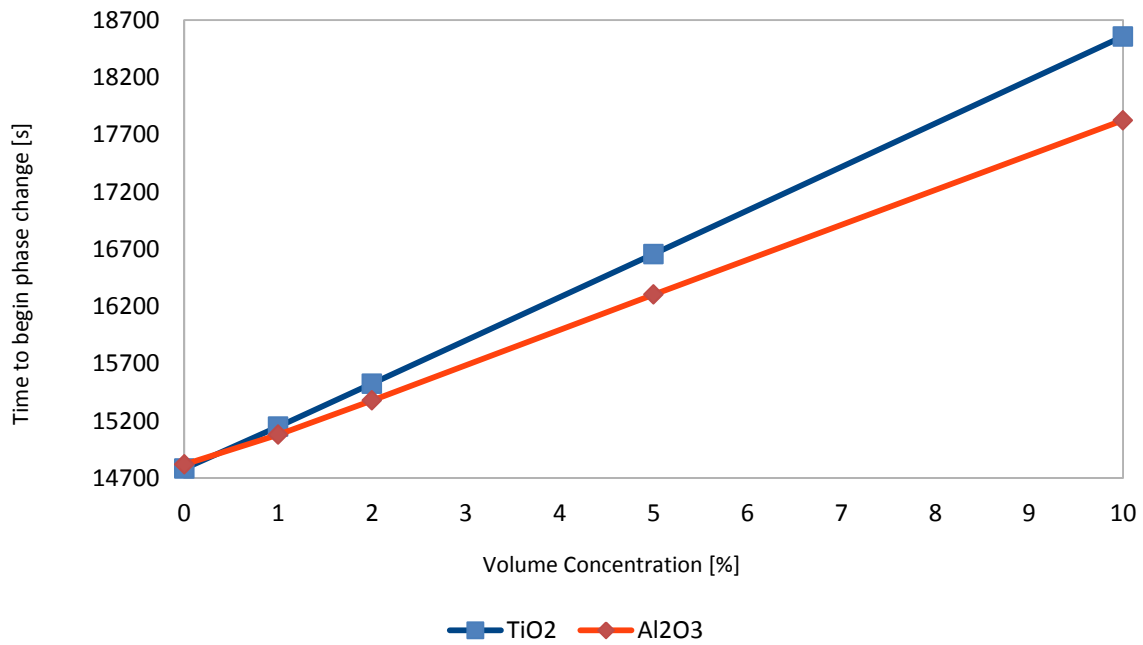**Fig. 7** Nusselt number for different volume concentrations of nanoparticles (CFD)

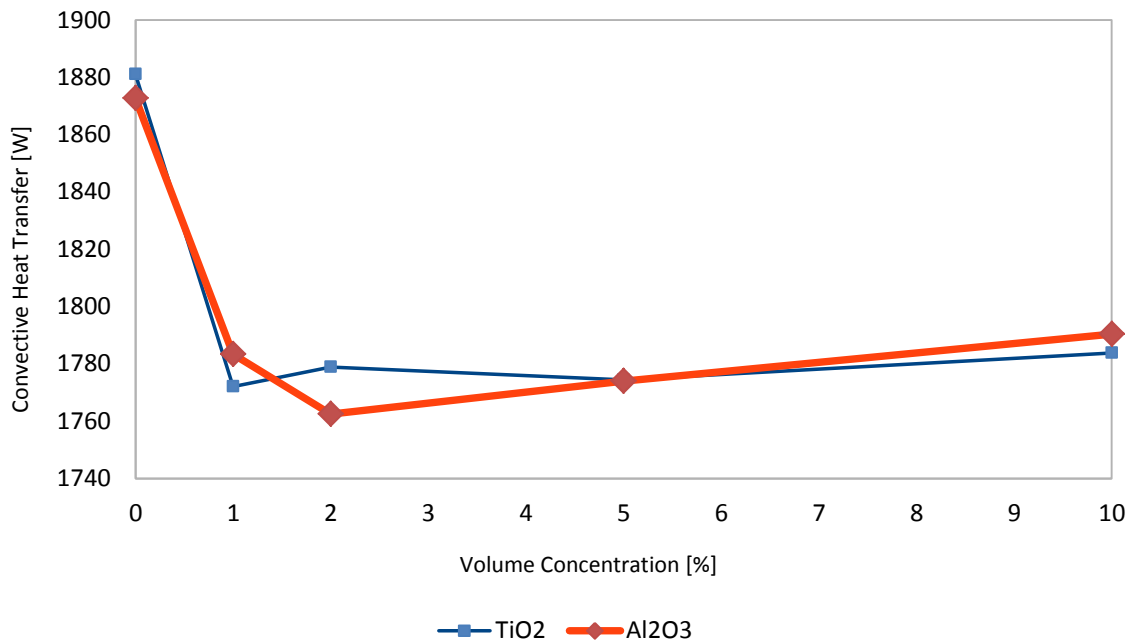**Fig. 8** Time to begin phase change for different volume concentrations of nanoparticles (TRAC-U)

Fig. 9 Convective heat transfer for different volume concentrations of nanoparticles (TRAC-U)
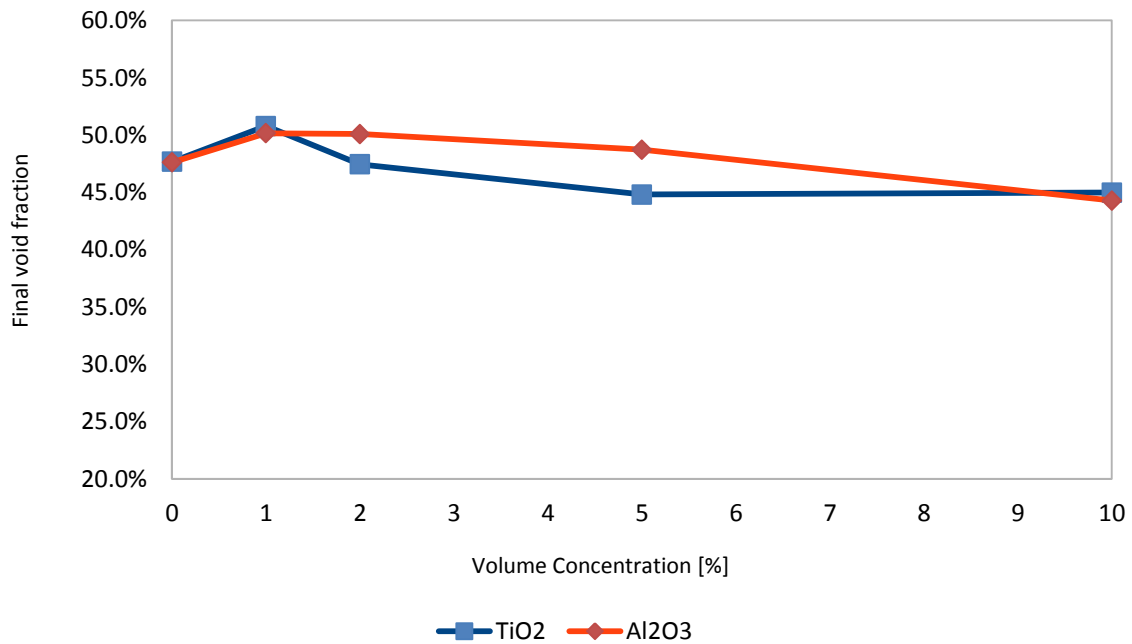

Fig. 10 Final void fraction for different volume concentrations of nanoparticles (TRAC-U)

4. Conclusions

A brief review of the nanofluids dynamics and modeling approach during pool boiling was performed. TRAC-U was introduced as a systematic and ongoing attempt to incorporate new developments into TRAC-BF1. The following aspects were studied in this paper through the implementation of TiO_2 and Al_2O_3 nanofluids: (a) The nanofluids impact in heat transfer mechanisms due to convection and conduction effects using the optimized model developed for chapter 1. (b) The nanofluids impact during phase change using a model developed in TRAC-U.

The major findings are: (1) When the dominant mechanism of heat transfer is a combination of convection and conduction the CFD model predicts an enhancement in the convective HTC when water is substituted with a nanofluid as the refrigerant in the system, with a maximum increment of 11% for TiO_2 and 13%. for Al_2O_3 (2) When phase change is occurring the TRAC-U model does not predict an enhancement in the convective heat transfer, with a maximum reduction of 6%, independent of the nanofluid used. (3) Density appears to be the most significant parameter in both models considering the five properties modified in the implementation of nanofluids.

References

[1]   J. S. Coursey and J. Kim, "Nanofluid boiling: The effect of surface wettability," Int. J. Heat Fluid Flow, vol. 29, no. 6, pp. 1577–1585, Dec. 2008.

[2]   W. Yu and H. Xie, "A review on nanofluids: preparation, stability mechanisms, and applications," J. Nanomater., vol. 2012, p. 1, 2012.

[3]   X. Fang, Y. Chen, H. Zhang, W. Chen, A. Dong, and R. Wang, "Heat transfer and critical heat flux of nanofluid boiling: A comprehensive review," Renew. Sustain. Energy Rev., vol. 62, pp. 924–940, 2016.

[4]   D. Ciloglu and A. Bolukbasi, "A comprehensive review on pool boiling of nanofluids," Appl. Therm. Eng., vol. 84, no. Supplement C, pp. 45–63, Jun. 2015.

[5]   E. Forrest, E. Williamson, J. Buongiorno, L.-W. Hu, M. Rubner, and R. Cohen, "Augmentation of nucleate boiling heat transfer and critical heat flux using nanoparticle thin-film coatings," Int. J. Heat Mass Transf., vol. 53, no. 1, pp. 58–67, 2010.

[6]   R.-H. Chen, T. X. Phuoc, and D. Martello, "Effects of nanoparticles on nanofluid droplet evaporation," Int. J. Heat Mass Transf., vol. 53, no. 19, pp. 3677–3682, 2010.

[7]   M. M. Ameen, K. Prabhul, G. Sivakumar, P. P. Abraham, U. B. Jayadeep, and C. B. Sobhan, "Molecular dynamics modeling of latent heat enhancement in nanofluids," Int. J. Thermophys., vol. 31, no. 6, pp. 1131–1144, 2010.

[8]   C. Y. Tso and C. Y. Chao, "Study of enthalpy of evaporation, saturated vapor pressure and evaporation rate of aqueous nanofluids," Int. J. Heat Mass Transf., vol. 84, pp. 931–941, 2015.

[9]   M. H. U. Bhuiyan, R. Saidur, M. A. Amalina, and R. M. Mostafizur, "Measurement of latent heat of vaporization of nanofluids using calorimetric technique," J. Therm. Anal. Calorim., vol. 122, no. 3, pp. 1341–1346, 2015.

[10]   S. Lee, P. E. Phelan, L. Dai, R. Prasher, A. Gunawan, and R. A. Taylor, "Experimental investigation of the latent heat of vaporization in aqueous nanofluids," Appl. Phys. Lett., vol. 104, no. 15, p. 151908, 2014.

[11]   S. Lee, R. A. Taylor, L. Dai, R. Prasher, and P. E. Phelan, "The effective latent heat of aqueous nanofluids," Mater. Res. Express, vol. 2, no. 6, p. 065004, 2015.

[12]   M. Chandrasekar, S. Suresh, and T. Senthilkumar, "Mechanisms proposed through experimental investigations on thermophysical properties and forced convective heat transfer characteristics of various nanofluids – A review," Renew. Sustain. Energy Rev., vol. 16, no. 6, pp. 3917–3938, Aug. 2012.

[13]   S.-Q. Zhou and R. Ni, "Measurement of the specific heat capacity of water-based Al 2 O 3 nanofluid," Appl. Phys. Lett., vol. 92, no. 9, p. 093123, 2008.

[14]   G.-J. Lee, C. K. Kim, M. K. Lee, C. K. Rhee, S. Kim, and C. Kim, "Thermal conductivity enhancement of ZnO nanofluid using a one-step physical method," Thermochim. Acta, vol. 542, pp. 24–27, 2012.

[15]   H. C. Brinkman, "The Viscosity of Concentrated Suspensions and Solutions," J. Chem. Phys., vol. 20, no. 4, pp. 571–571, Apr. 1952.

[16]   H. Chen, S. Witharana, Y. Jin, C. Kim, and Y. Ding, "Predicting thermal conductivity of liquid suspensions of nanoparticles (nanofluids) based on rheology," Particuology, vol. 7, no. 2, pp. 151–157, Apr. 2009.

[17]   James Clerk Maxwell, A Treatise on Electricity & Magnetism, 3rd ed., vol. 1. Clarendon Press, 1891.

[18]   B. Elhajjar, G. Bachir, A. Mojtabi, C. Fakih, and M. C. Charrier-Mojtabi, "Modeling of Rayleigh–Bénard natural convection heat transfer in nanofluids," Comptes Rendus Mécanique, vol. 338, no. 6, pp. 350–354, 2010.

[19]   S. K. Das, N. Putra, and W. Roetzel, "Pool boiling characteristics of nano-fluids," Int. J. Heat Mass Transf., vol. 46, no. 5, pp. 851–862, 2003.

[20]   D. Zhu, S. Wu, and N. Wang, "Thermal physics and critical heat flux characteristics of Al2O3–H2O nanofluids," Heat Transf. Eng., vol. 31, no. 14, pp. 1213–1219, 2010.

[21]   A. H. Harvey and E. W. Lemmon, NIST/ASME Steam Properties—STEAM. 2013.

[22]   R. S. Vajjha and D. K. Das, "Specific heat measurement of three nanofluids and development of new correlations," J. Heat Transf., vol. 131, no. 7, p. 071601, 2009.

[23]   R. S. Vajjha and D. K. Das, "Experimental determination of thermal conductivity of three nanofluids and development of new correlations," Int. J. Heat Mass Transf., vol. 52, no. 21, pp. 4675–4682, 2009.

[24]   H. K. Dawood, H. A. Mohammed, N. A. C. Sidik, and K. M. Munisamy, "Numerical investigation on heat transfer and friction factor characteristics of laminar and turbulent flow in an elliptic annulus utilizing nanofluid," Int. Commun. Heat Mass Transf., vol. 66, pp. 148–157, 2015.

[25]   A. A. Minea and O. Manca, "Field-Synergy and Figure-of-Merit Analysis of Two Oxide–Water-Based Nanofluids' Flow in Heated Tubes," Heat Transf. Eng., vol. 38, no. 10, pp. 909–918, 2017.

[26]   F. Garoosi, L. Jahanshaloo, M. M. Rashidi, A. Badakhsh, and M. E. Ali, "Numerical simulation of natural convection of the nanofluid in heat exchangers using a Buongiorno model," Appl. Math. Comput., vol. 254, pp. 183–203, 2015.

[27]   T. L. Bergman, A. S. Lavine, F. P. Incropera, and D. P. Dewitt, Fundamentals of heat and mass transfer. John Wiley & Sons New York, 2011.

[28]   J. A. Borkowski et al., "TRAC-BF1/MOD1: An advanced best-estimate computer program for BWR accident analysis, Model description. Volume 1," Nuclear Regulatory Commission, Washington, DC (United States). Div. of Systems Research; Idaho National Engineering Lab., Idaho Falls, ID (United States), 1992.

[29]   W. H. McAdams, Heat Transmission: 3d Ed. McGraw-Hill, 1954

Comparative Analysis of Different Configurations
to Enhance the ESBWR Passive Cooling Systems

Abstract

In the present study the results from chapter 1 and chapter 2 as well as an additional set of first principles experiments are used to draw conclusions about possible enhancements to the ESBWR passive cooling systems. It is found that losing coolant by evaporation is preferable over a pool with a near-complete inventory at higher temperature. A passive TPCT cooled by air that removes decay heat while conserving the water inventory of the PCCS pools coupled with a shroud favoring the phase change around the heat exchangers seems like the optimal alternative to enhance the ESBWR passive cooling systems. Limiting cases probably bounding the PCCS actual response when adding nanofluids are identified.

Keywords: ESBWR, Passive cooling systems, Nanofluids, TPCT, ROM, CFD, TRAC-U

1. Introduction

The Economic and Simplified Boiling Water Reactor (ESBWR) is a generation 3+ boiling water reactor with a net electric output of 1520 Mw_e(GEH, [1]). The core is cooled by a flow rate driven by natural circulation of 9600 $\frac{kg}{s}$, producing 2400 $\frac{kg}{s}$of steam approximately (GEH, [2]). Other key design characteristics can be found in Table 1. The main compartments inside the vessel and its corresponding volume are shown in Figure 1.

Table 1 ESBWR key design characteristics (GEH, [2])

Parameter	Unit	Value	Parameter	Unit	Value
Rated power	MW_t	4500	Fuel rod array	—	10 × 10
Operating pressure	MPa	7.17	Fuel rods per assembly	—	92
Average core power density	$\frac{kW}{l}$	54.3	Overall length	m	3.79
Maximum linear heat generation rate	$\frac{kW}{m}$	44.0	Weight of UO_2 per assembly	kg	163
Average linear heat generation rate	$\frac{kW}{m}$	15.1	Rod diameter	cm	1.026
Core average exit quality	%	25	Fuel channel dimensions	cm	14 × 14
Feedwater temperature	$°C$	215.6	Reactor power control	—	Control rods. Feedwater temperature
Fuel assemblies	—	1132	Vessel inside diameter	m	7.1
Control rods	—	269	Vessel inside height	m	27.6

The ESBWR has at its disposal 6 different passive safety systems[25] (GEH, [3], Fig. 2) consisting of the Isolation Condenser System (ICS), the Passive Containment Cooling System (PCCS), the Gravity Driven Cooling System (GDCS), the Automatic Depressurization System (ADS), the Basemat Internal Melt Arrest and Coolability (BiMAC) and the Standby Liquid Control System (SLCS).

The BiMAC is a core catcher designed to quench the high temperature mixture of materials in the event of a nuclear meltdown. The SLCS is designed to shutdown the reactor by injecting

---

[25] The GDCS, ADS, SLCS and BiMAC are actually initiated by DC power.

nitrogen-driven boron. Both systems provide backup in the case the other passive systems are unable to function.

The objective of the remaining passive systems is to prevent core overheating maintaining the temperature at or below the normal operating value. In the event of a pipe leak or break a SCRAM would be triggered with the feedwater keeping a sufficient water level.
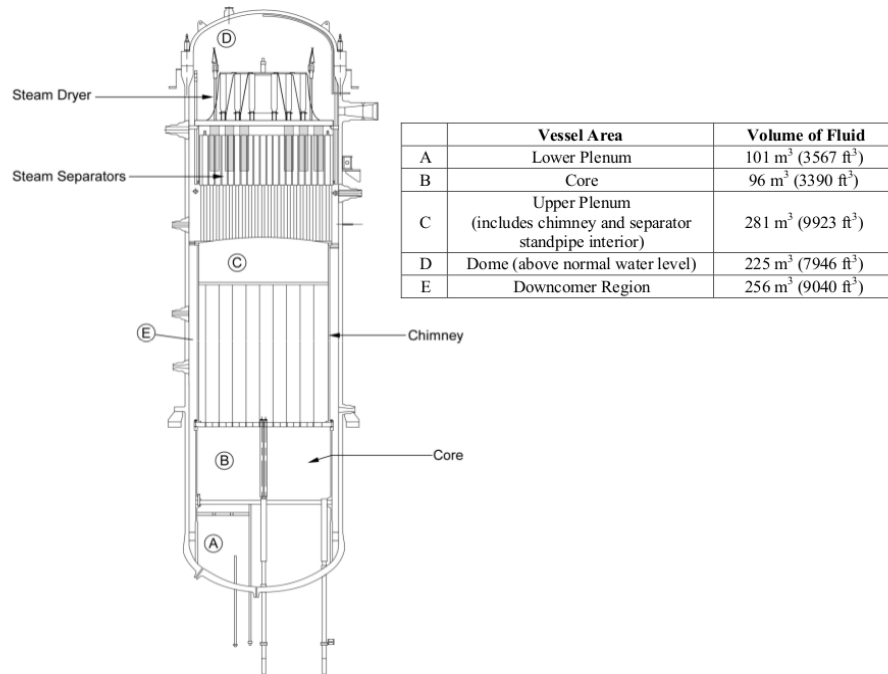

	Vessel Area	Volume of Fluid
A	Lower Plenum	101 m^3 (3567 ft^3)
B	Core	96 m^3 (3390 ft^3)
C	Upper Plenum (includes chimney and separator standpipe interior)	281 m^3 (9923 ft^3)
D	Dome (above normal water level)	225 m^3 (7946 ft^3)
E	Downcomer Region	256 m^3 (9040 ft^3)

Fig. 1 ESBWR main compartments inside the vessel (GEH, [4])

In the case the pipe leak or break occurs simultaneously with a station blackout the IC would start by draining the water in its tubes into the vessel to draw steam into the heat exchangers (Table 2) submerged in the upper pools of the building cooling the reactor.

Table 2 Upper pool heat exchangers capacity (GEH, [5])

Parameter	Unit	Value
ICS units	—	4
ICS Capacity (Single unit)	MW	33.75
ICS Capacity (Total)	MW	135
PCCS units	—	6
PCCS Capacity (Single unit)	MW	11
PCCS Capacity (Total)	MW	66

If the level drops below an anticipated operational occurrence a depressurization sequence begins by opening the Safety Relieve Valves (SRV) transferring steam into the suppression pool, followed by the activation of the Depressurization Valves (DPV) transferring steam into the dry well. At the end of depressurization the GDCS starts its operation raising the water level.

At this point the PCCS begins by drawing the steam in the drywell into a different set of heat exchangers (Table 2) also submerged in the upper pools of the building and draining the condensate into the GDCS, cooling the reactor for at least 72 hours until the water in the upper pools is evaporated without operation action (GEH, [4]).
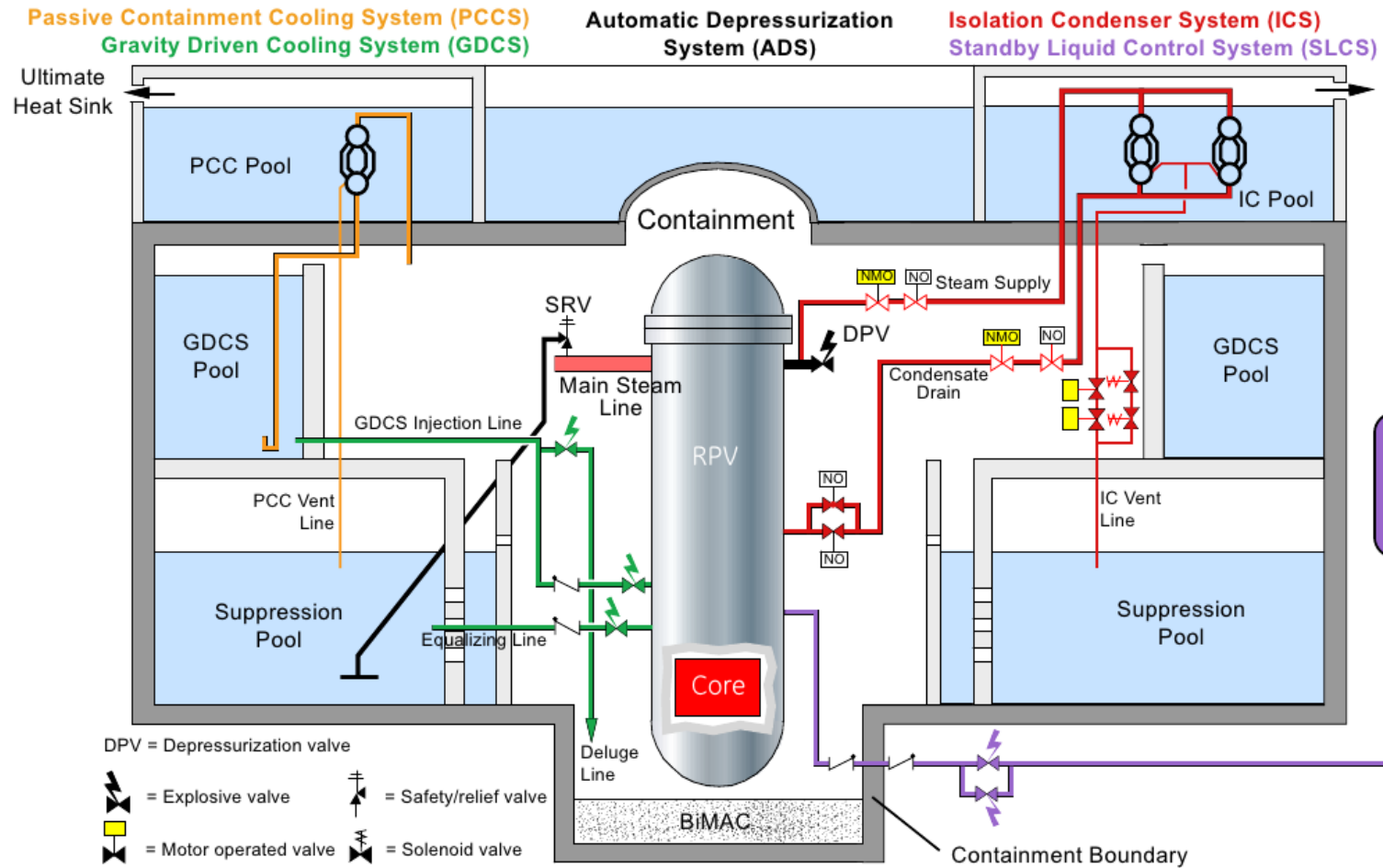
Fig. 2 ESBWR key safety systems (GEH, [2])

2. Methods

The current analysis will be limited to the upper pools passive systems (PCCS and ICS) even though the GDCS works in conjunction with the PCCS. The GDCS pools drain into the vessel and therefore they are not planned to be augmented with nanoparticles until the possible neutronic interactions are clearly established. Furthermore the analysis will be focused in the PCCS due to its involvement in the long-term response of the system.

The models developed for chapter 1 and chapter 2 as well as an additional set of first principles experiments will be used to draw conclusions about possible enhancements to the ESBWR passive cooling systems.

The system used in the first configuration of chapter 1 was designed to be a representation in scale 1:500 in volume of one of the emergency pools of the passive containment cooling system (PCCS) of a simplified and economic boiling water reactor (ESBWR).

According to the company behind its development, GE-Hitachi, the system has the purpose of "limit containment pressure to less than its design pressure for at least 72 hours after a loss of coolant accident (LOCA) without water makeup to the pool, and beyond 72 hours with pool makeup and vent fan operation" (GEH, [2])

The construction of the ESBWR has not yet begun, and as a consequence the PCCS pools configuration may vary, but as committed by GE-Hitachi, they will have a combined volume of no less than 6,290 m³ (GEH, [6]). Therefore the lower end capacity for a single cavity of the PCCS should be around 100 m³, setting the volume of the scaled system to 0.2 m³.

The power that the PCCS have to dissipate corresponds to the nuclear reactor decay heat, which is a function of the operating power and time after shutdown. In the ESBWR case with a rated thermal power of 4500 MW, the decay is approximately 51 MW one hour after shutdown, and one third of that value after 72 hours.

Nevertheless, with the purpose of performing a conservative analysis and assuming the total volume available in the pools is used to cool down the nuclear system, the decay heat fraction

corresponding to a single PCCS cavity is considered constant during the case study at a value of 800 kW. In this way, a submerged electrical resistance with an approximate power of 1600 W was used as a source to maintain the power-volume ratio of the real system.

With respect to the emergency pools of the passive containment cooling system, the 72 hours design commitment for cooling without makeup to the pool corresponds with a conservative estimation that contemplates evaporating only 50 % of the available liquid volume. Hence the claim that passive safety provides more than 7 days of reactor cooling without AC electrical power or human action (GEH, [3]).

The surface to volume ratio in the second configuration of chapter 1 is two orders of magnitude higher than in the emergency system pools, resulting in an evaporation rate three times as fast in comparison with the commitment for the real system. Nevertheless, in the larger-scale case where the surface to volume ratio is more similar, the evaporation rate matches the estimate made by the reactor designer.

The CFD model used in chapter 2 was taken directly from chapter 1. The purpose was to analyze the response of a scaled PCCS system augmented with nanofluids with a focus in convection and conduction heat transfer mechanisms. The TRAC-U model supplemented this analysis with a two phase 1D-transient model based on TRAC-BF1 routines by considering a configuration equivalent to a single tube in the PCCS pool.

A set of first principles experiments was conducted to gain insight into the effects in the evaporation rate of different passive cooling systems configurations. The experiments were an extension of the boundary conditions studied in chapter 1 employing a smaller-scale system similar to the 0.6 dm³ used in that study. The power density was 1000 $\frac{kW}{m^3}$with a duration of 500 [s] in all cases. The additional boundary conditions included (1) a chimney on top of the water-air interface, (2) an open conical lid partially obstructing the evaporation flow, (3) the combination of the previous two cases, (4) a shroud around the submerged power source and (5) an open surface case as reference.

3. Results and discussion

The experimental data from chapter 1 shows that losing coolant by evaporation is preferable over a pool with a near-complete inventory at higher temperature and therefore less capacity to cool the heat source.

The shroud case (Fig. 3) modeled using the ROM model (Fig. 3) appears to enhance the removal of heat by not allowing the redistribution of energy through convection, leading to a faster loss of coolant inventory. On the other hand, the Two Phase Closed Thermosyphon (TPCT) case shows that a second passive loop can provide a prolonged and stable heat removal capacity if a configuration capable of transferring heat and not mass outside the containment is devised.
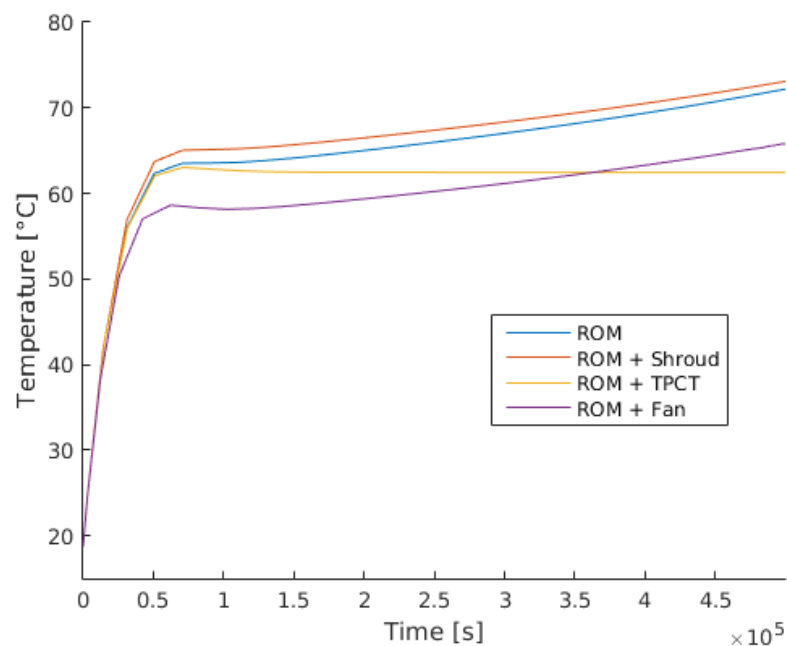

Fig 3. Long-term response predictions estimated using the Reduced Order Model (Chapter 1)

The CFD model from chapter 2 predicts an enhancement in the response of the PCCS by adding nanofluids when only convection and conduction effects are considered. Conversely, the TRAC-U model establishes a deterioration in heat transfer by adding nanofluids when the phase change is considered explicitly (Fig. 4). However, the heat transfer occurring in the PCCS is a 3D phenomenon, and therefore supplementary studies are required before ruling them out or accepting them as an alternative to enhance the ESBWR passive cooling systems. The CFD and TRAC-U results are probably the limiting cases bounding the PCCS actual response when adding nanofluids.
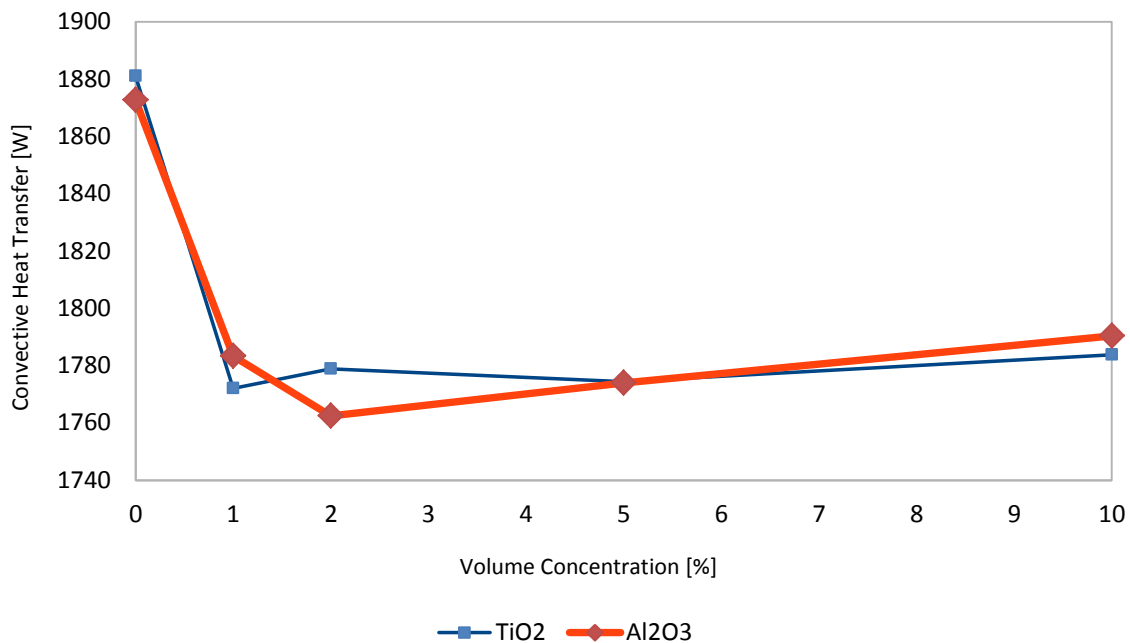

Fig 4. Convective heat transfer for different volume concentrations of nanoparticles (Chapter 2)

The additional set of experiments indicate that the effect of the configuration evolves as the global temperature approaches saturation. At the very beginning, all configurations behave similarly due to the dominant effect of convection. Once the bubbles have enough energy to escape the air-water surface, the configuration's effect becomes apparent by modifying the phase change dynamics.

Both the open conical cover and the chimney act as restrictions to the flow by interfering with the diffusion of vapor, increasing the local temperature of air above the surface and promoting boiling. The open conical cover and the chimney also act as condensation surfaces, recovering a fraction of the lost fluid.

The flow restriction and condensation are competing effects, but it seems that when the open conical cover is close to the air-surface the restriction effect is dominant, while the condensation effect is prevalent when the open conical cover is mounted on top of the chimney (Table 3).

Table 3. First principles experiments: Remaining mass

Configuration	Remaining mass g
Open conical cover	465.0
Open surface	469.1
Chimney alone	474.5
Chimney + Open conical cover	481.7

The first principles experiment were designed to amplify the effect of the different configuration by running at a higher power density than the PCCS. However, the experiments clearly confirm the findings from the ROM model related to the shroud effect (Fig 5).
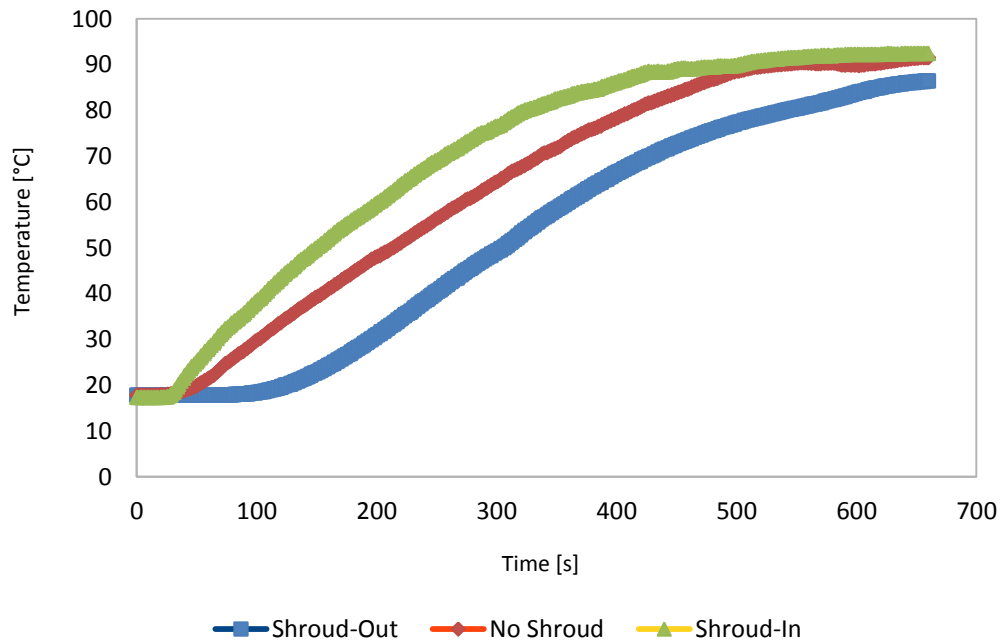

Fig. 5 First principles experiments: Shroud effect

A passive TPCT cooled by air that removes decay heat while conserving the water inventory of the PCCS pools coupled with a shroud favoring the phase change around the heat

exchangers seems like the optimal alternative to enhance the ESBWR passive cooling systems.

4. Conclusions

A brief review of the ESBWR characteristics and configuration was performed. The results from chapter 1 and chapter 2 as well as an additional set of first principles experiments were used to draw conclusions about possible enhancements to the ESBWR passive cooling systems.

The major findings are: (1) Losing coolant by evaporation is preferable over a pool with a near-complete inventory at higher temperature and therefore less capacity to cool the heat source. (2) Limiting cases probably bounding the PCCS actual response when adding nanofluids are identified. (3) A passive TPCT cooled by air, that removes decay heat while conserving the water inventory of the PCCS pools coupled with a shroud favoring the phase change around the heat exchangers, seems like the optimal alternative to enhance the ESBWR passive cooling systems.

References

[1]   GEH, "ESBWR Nuclear Power Plant," Jan-2017. [Online]. Available: https://nuclear.gepower.com/build-a-plant/products/nuclear-power-plants-overview/esbwr.

[2]   GEH, ESBWR Plant General Description. General Electric Hitachi Nuclear Energy, 2011.

[3]   GEH, "ESBWR Passive Safety Fact Sheet." 2011.

[4]   GEH, "ESBWR Design Control Document," Tier 2, Chapter 5: Reactor Coolant System and Connected Systems, 2014.

[5]   GEH, "ESBWR Design Control Document," Tier 2 Chapter 6: Engineered Safety Features, 2014.

[6]   GEH, "ESBWR Design Control Document," Tier 1, 2013.

Conclusions

The following aspects were studied in chapter 1 titled **"Estimation Of Heat Transfer Mechanisms In Heated Water Bodies Using A Reduced Order Model Assisted By Computational Fluid Dynamics"**: The long-term spatial and temporal transient response of a system involving boiling and evaporation as well as conduction and convection due to a localized heat source in terms of power dissipation and mass loss using a combined ROM-CFD analysis. The distinction between water evaporation and boiling using the power density as a figure of merit to determine the most appropriate approach to quantify mass and energy long- term evolution in heated water bodies.

The major findings in chapter 1 are: (1) The heat transfers through the water-air surface with or without mass transport are the most significant dissipation mechanisms throughout the present study. When these mechanisms are inhibited by adding a lid, the temperature of the system increases its tendency to reach saturation, but even in that case the system temperature stabilizes below saturation due the low power density. (2) When the heat source power density is less than 100 kW/m³, a simple evaporation analysis becomes a viable approach to approximate the long-term behavior of the real system.

In chapter 2 titled **"TRAC-U – CFD Analysis of Nanofluids in Heated Water Bodies"** a brief review of the nanofluids dynamics and modeling approach during pool boiling was performed. TRAC-U was introduced as a systematic and ongoing attempt to incorporate new developments into TRAC-BF1. The following aspects were studied in this section through the implementation of TiO_2 and Al_2O_3 nanofluids: (a) The nanofluids impact in heat transfer mechanisms due to convection and conduction effects using the optimized model developed for chapter 1. (b) The nanofluids impact during phase change using a model developed in TRAC-U.

The major findings in chapter 2 are: (1) When the dominant mechanism of heat transfer is a combination of convection and conduction the CFD model predicts an enhancement in the convective HTC when water is substituted with a nanofluid as the refrigerant in the system, with a maximum increment of 11% for TiO_2 and 13%. for Al_2O_3 (2) When phase change is

occurring the TRAC-U model does not predict an enhancement in the convective heat transfer, with a maximum reduction of 6%, independent of the nanofluid used. (3) Density appears to be the most significant parameter in both models.

In chapter 3 titled **"Comparative Analysis of Different Configurations to Enhance the ESBWR Passive Cooling Systems"** a brief review of the ESBWR characteristics and configuration was performed. In this chapter the results from chapter 1 and chapter 2 as well as an additional set of first principles experiments were used to draw conclusions about possible enhancements to the ESBWR passive cooling systems.

The major findings in chapter 3 are: (1) Losing coolant by evaporation is preferable over a pool with a near-complete inventory at higher temperature and therefore less capacity to cool the heat source. (2) Limiting cases probably bounding the PCCS actual response when adding nanofluids are identified. (3) A passive TPCT cooled by air that removes decay heat while conserving the water inventory of the PCCS pools coupled with a shroud favoring the phase change around the heat exchangers seems like the optimal alternative to enhance the ESBWR passive cooling systems.